MASTER'S THESIS

CONTROLLED MORPHOLOGY EVOLUTION OF PLA VIA RAPID HEAT CYCLE MOLDING

by

THOMAS HUTTERER

Montanuniversität Leoben

Department of Polymer Engineering and Science

Chair of Injection Molding of Polymers

Supervision: Ass.Prof. Dipl-Ing. Dr. mont Gerald Berger

DI Dr.mont. Gernot Pacher

Assessment: Univ.-Prof. DI Dr.mont. Walter Friesenbichler

EIDESSTATTLICHE ERKLÄRUNG

Ich erkläre an Eides statt, dass ich die vorliegende Masterarbeit/Bachelorarbeit selbständig und ohne fremde Hilfe verfasst, andere als die angegebenen Quellen und Hilfsmittel nicht benutzt und die den benutzten Quellen wörtlich und inhaltlich entnommenen Stellen als solche erkenntlich gemacht habe.

AFFIDAVIT

I declare in lieu of oath, that I wrote this thesis and performed the associated research myself, using only literature cited in this volume.

Leoben, September 2016

Acknowledgement

First of all, I want to thank my assessor Univ.-Prof. DI Dr.mont Walter Friesenbichler for enabling me to realize this master's thesis in cooperation with the Chair of Injection Moulding of Polymers and I want to thank him for his thorough and fair assessment of my work.

Furthermore I want to thank my supervisors Ass. Prof. DI Dr. mont Gerald Berger and DI Dr. mont. Gernot Pacher for their support and supervision throughout the process of research and I especially want to thank DI Dr. mont. Gernot Pacher for providing me guidance on new subjects as well as being always available for feedback.

The research work of this paper was performed at the Polymer Competence Center Leoben GmbH (PCCL, Austria) within the framework of the COMET-program of the Federal Ministry for Transport, Innovation and Technology and the Federal Ministry of Science, Research and Economy with contributions by the Department of Polymer Engineering and Science at Montanuniversität Leoben. The PCCL is funded by the Austrian Government and the State Governments of Styria, Lower Austria and Upper Austria.

A substantial amount of this work was also done in cooperation with the Chair of Material Science and Testing of Polymers, and I want to thank Univ.-Prof. DI Dr. mont. Gerald Pinter for being able to work with the equipment of this chair as well as Walter Rath and Florian Arbeiter for guidance.

I also want to mention Eduard Leitner, Ivica Duretek, Astrid Rauschenbach, and Wolfgang Ziegler, which all provided their expertise on subjects critical to this work.

Additionally I want to give my regards to my colleagues at the PCCL and my fellow students, which provided me help through showing me different approaches and being open for discussions on my work.

Last but not least, I want to thank my parents for enabling my studies and always showing me their deepest support.

Abstract

Due to the ever-growing demand of biobased polymers, ways to increase their applicability as technical parts need to be established. Poly (lactic acid) is by now the most widely used biopolymer, but its improper crystallization behaviour when processed via injection molding limits its usefullness to a great degree.

In this work, two approaches to increase the degree of crystallinity of PLA parts with state of the art injection moulding equipment are being proposed. First, compounds of PLA and nucleating agents, specifically talc and layered silica, were made, and secondly, specimens were manufactured from those compounds using Rapid Heat Cycle Molding (RHCM) process control during injection molding. The injection moulding experiments were carried out according to a full factorial Design of Experiments (DOE) for every compound.

The manufactured specimens were then analysed with Differential Scanning Calorimetry (DSC) in order to obtain the achieved degree of crystallinity by the different compounds and DOE settings. Furthermore, polarized optical micrographs were made to investigate the distribution of crystallites across the diameter of the samples. Lastly, hardness measurements were carried out.

The results of the DSC measurements were then statistically analysed and models were fit to the data. The fits of the different materials were then compared to analyse the effect of nucleation separately from the effectiveness of the RHCM process. Those results were then linked to the polarized optical micrographs and hardness measurements.

It was shown that adding talc to PLA can increase the degree of crystallinity achieved during injection moulding considerably, even at low RHCM temperatures. Furthermore, talc greatly enhances the distribution of crystallites across the part diameter as opposed to the raw material, which only shows crystallites close to the heated cavity walls. Furthermore, Shore D Hardness measurements proved to be a quick and easy method to compare the different degrees of crystallinity within the same material.

Zusammenfassung

Der Bedarf an biobasierten Kunststoffen steigt weltweit immer noch stetig an, weswegen Wege gefunden werden müssen, um diese Polymerklasse auch für die Anwendung als technische Bauteile interessant zu machen. Polymilchsäure (PLA) stellt den wichtigsten Vertreter der Biokunststoffe dar, ihre Anwendung ist jedoch stark durch ihre schlechten Kristallisationseigenschaften im Spritzgussprozess begrenzt.

In dieser Arbeit werde zwei Zugänge vorgestellt, die die Kristallinität von PLA- Bauteilen bei klassischer Verarbeitung erhöhen sollen. Als erstes wurden Compounds mit PLA und Nuklierungsmittel, im Speziellem Talk und Schichtsilikat, hergestellt, und diese wurden dann auf einer Spritzgussmaschine mit variothermer Prozessführung verarbeitet. Jeder der Compounds wurde mit Hilfe eines Versuchsplans zu Probekörpern verarbeitet.

Diese Probekörper wurden mittels dynamischer Differenzkalorimetrie (DSC) analysiert, um die im Verarbeitungsprozess erreichten Kristallinitätsgrade zu bestimmen. Zusätzlich wurden Mikroskopieaufnahmen unter polarisiertem Licht angefertigt, um die Verteilung der Kristallite über den Probenquerschnitt zu untersuchen. Zuletzt wurden auch Härtemessungen durchgeführt.

Die Ergebnisse der DSC Messungen wurden statistisch ausgewertet und an die Daten wurden Modelle gefittet. Die Modelle, die sich für die unterschiedlichen Materialien ergaben, wurden verglichen, um den Effekt der Nukleierungsmittel von dem der variothermen Prozessführung trennen zu können. Diese Ergebnisse wurden anschließend mit den Mikroskopieaufnahmen und der Härtemessung in Kontext gesetzt.

Es konnte so gezeigt werden, dass Talk den Kristallinitätsgrad von PLA während des Spritzgießens signifikant erhöhen kann, auch wenn nur wenig dynamische Werkzeugtemperierung eingesetzt wird. Zusätzlich führt der Einsatz von Talk zu einer merklich gleichmäßigeren Verteilung der Kristallite über den gesamten Probenquerschnitt. Es konnte auch gezeigt werden, dass die Härte nach Shore D eine schnelle Vergleichsmöglichkeit hinsichtlich unterschiedlicher Kristallinitäten im selben Material bietet.

Contents

1 Introduction

1.1 Motive

Biologically based biopolymers are highly demanded by the market as well as by society. However, their use in real world applications is still very limited, due to two major limiting factors. One is the higher price of biologically based polymers compared to commodity plastics [1]. The other, a rather small amount of industry research has been done regarding the property modification of biopolymers during processing. As will be shown in section 2.2, there is a broad base of knowledge on what can raise mechanical and other properties of PLA. However, fewer studies have been carried out on how to achieve these modifications under processing conditions [2, 3]. The goal of this work is to use talc and nanoclay filled polylactic acid for injection moulding processing and to investigate the favorable crystallization dynamics of these compounds under manufacturing conditions (section 2.2, section 2.3). By employing a dynamically temperature controlled mould, annealing of the produced parts can be achieved, while active cooling after the heating cycle reduces additional cycle time. By creating temperatures around the crystallization temperature, changes in degree of crystallinity as well as crystalline structure of the polymer are expected. These changes will be investigated by Differential Scanning Calorimetry (DSC) analysis as well as by optical micoscropy. This procedure is expected to increase the understanding on how to achieve higher levels of properties within PLA nanocompound-based products and thus enable a more widespread use of these types of materials.

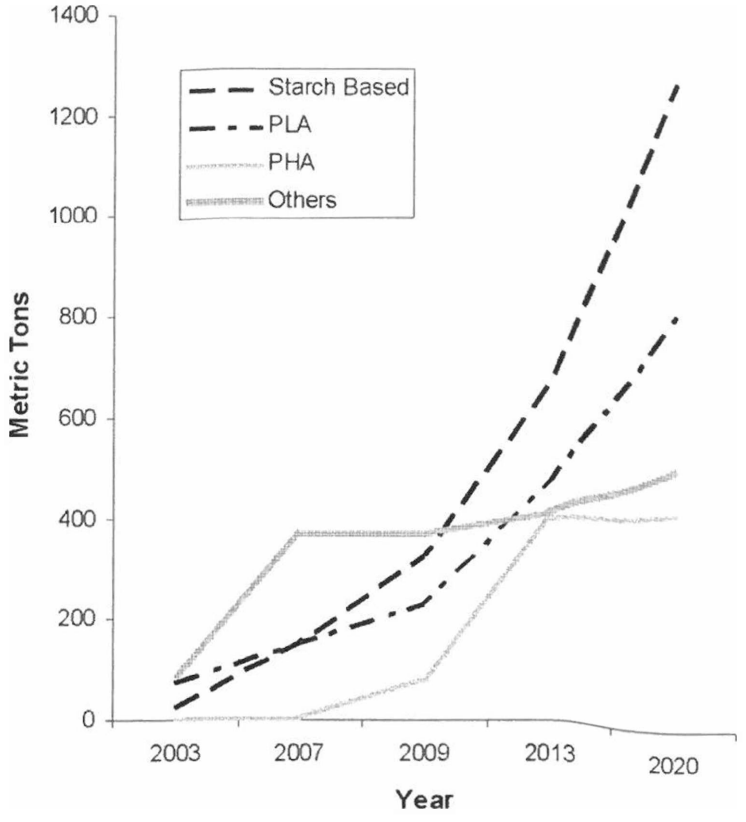

Figure 1.1: World production volume of biopolymers (estimated from 2009 onwards) [1].

1.2 Market Situation

The ability to cheaply mass-produce commodity polymers, mainly polyethylene (PE), polypropylene (PP) , polystyrene (PS) and polyvinylchloride (PVC) has caused an abundant use of those materials among all possible applications. By 2011, world wide plastic demand has reached an all time high of 235 million tons, with Europe alone using up to 22% of this number accounting to 47 million tons [4]. Figure 1.1 shows the world production mass of biopolymers with estimated values from 2003 onwards.

The aforementioned polymers are mainly produced from non-renewable resources, often employing by-products of oil refinement as basic components for the synthesis of chemical substances later used for polymer synthesis [5]. There are, however two main trends leading

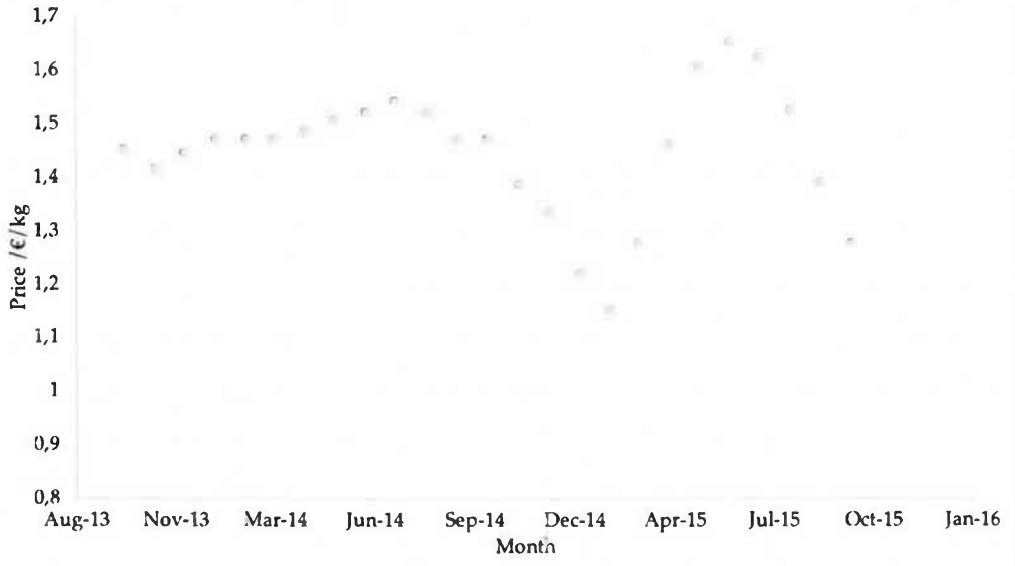

Figure 1.2: Fluctuation of recent polypropylene homopolymer prices over 48 months [7].

to a demand for non-petrochemically based plastics. First, there is an ever growing awareness in society of the ecological impact our lifestyle has on the environment. This means politicians exert increasing pressure on manufacturers to steadily lower the energy consumption of their production processes and products [6]. Furthermore, consumers are also demanding products that do have a smaller ecological footprint and cause less environmental pollution and CO_2 emissions [5]. Second, by being largely based on crude oil, plastic prices are almost directly connected to oil price, which is subject to many factors, including speculation, which causes a high price volatility which is directly passed on to polymer prices. Manufacturers of plastic products, however, are only able to pass on price fluctuation to their custumers to a limited amount. This also places a higher risk on long term contracts and price guarantees. To illustrate this, Figure 1.2 shows recent price changes over 48 months per one kilogram of polypropylene homopolymer. Because of these two trends, there is money to be gained for manufacturers by stepping up their commitment to fade out the use of petrochemically based polymers and introduce polymers based of renewable resources [5].

1.3 Types of Biopolymers

With polymers known under the group name of biopolymers, one can distinguish different property based subgroups by which these can be separated, as shown in Figure 1.3. Among them, the three most important ones should be described further:

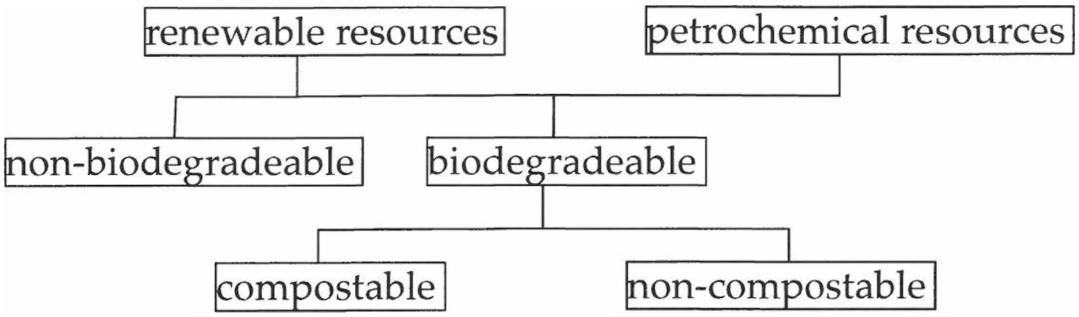

Figure 1.3: Schematic of types of biopolymers.

The first subgroup consists of biodegradable, but petrochemically based polymers. These polymers are - in strong contrast to common polymer modification practice - designed to show a low resistance to environmental influences [5, 8]. Noteworthy polymer types of this category are polycaprolactones (PCL) and polyvinylalcohols (PVA) . Since they are still based on byproducts of the cracking process of petroleum, these polymers do only solve the problems mentioned in chapter 1 to a limited degree.

The second subgroup consists of polymers which are based on renewable resources such as starch, proteins or plant oils, but are not biodegradeable [1, 8]. The polymer types produced are often well-known types of plastics such as PE, PP and polyethylene terephthalate (PET) . However, with these types of polymers, not environmental concerns are the key selling point but much rather considerations regarding availability and pricing of the starting materials. This category makes up the majority of global biopolymer production, accounting to around 62% of the 2013 total production of 1,62 million tons [9]. Often, synthesis of these polymers is conducted very similarly to their petroleum based counterparts in order to be able to switch between source materials with little effort. This can balance availability problems occuring with specific resources [5, 10]. The third subgroup, to which many people actually refer to

by using the term biopolymers, are polymers based on renewable resources which are also biodegradeable. In this thesis, the most prominent representative of this group, poly(lactic acid) (PLA) is being used.

Biological degradation of -but not limited to- polymers can be separated into two stages, 1) primary degradation- the division of the polymeric chain into smaller portions and 2) final degradation- the conversion of these to water, carbon dioxide or biomass [5]. Various factors contribute to the degradation of polymers. First, polymer structure is to be mentioned. Polymers posessing hydrolyzable structures in their backbones are most prone to degradation, with stereochemical effects (chirality) hindering or enhancing decomposition [8]. Second, polymer morphology plays an important role, since crystalline sections render hydrolyzable groups within the polymer chain unaccessible to enzymes. Thus, higher crystallinity can lead to elongated degrading times [11]. Also the exposure to radiation and chemical treatment and the molar mass are important influences in decomposition [8].

2 Theoretical Background

2.1 Crystallization in Polymers

In this section, basic and general research on the crystallization mechanisms in semicrystalline polymers is summarized. Special focus is being put on mechanisms also occuring during the crystallization of PLA, while other aspects are not treated extensively, in order to keep this section as lean as possible.

2.1.1 Primary Nucleation of Polymer Crystals

Crystalline areas of polymers are defined as areas within the material where chain segments of different molecules are aligned, forming intra- and intermolecular superstructures. Polymers can crystallize under different circumstances. Crystallization can already occur during polymerization, while orientation effects, e.g. caused by outside forces, can lead to the formation of Shish-Kebab structures, which are explained in subsection 2.1.5 [12]. In this chapter however, bulk crystallization from the melt is being explained further, since this mechanism can be expected to occur during injection moulding processing. Generally, crystallization starts at so-called nuclei, which are formed when the temperature of the polymer traverses its crystallization temperature T_c . There are two types of nucleation. First, homogenous nucleation occurs when small local fluctuations in density cause temporary alignments of very short chain segments. With increasing supercooling of the melt, the number of aligned segments needed to form a nucleus decreases. For most of the time, these nuclei do not cause any wide area phase changes. However, since crystallization follows the second law of thermodynamics,

the Gibbs free energy function, which characterizes the energy release or absorption of Gibbs free energy by a system, can lead to understanding which circumstances make nuclei grow to crystals. The Gibbs free energy function is given by [13]:

$$\Delta G = \Delta H - T\Delta S \tag{2.1}$$

where

ΔG = change in Gibbs free energy

ΔH = change in enthalpy

T = Temperature

ΔS = change in entropy

For crystallites to be formed within polymers, the crystallized state must be energetically favorable compared to the amorphous state, which causes a release of Gibbs free energy at the time of phase transition. Under the assumption of spherical crystallites, ΔG is also given by:

$$\Delta G = \frac{4}{3} * \pi * r^3 * \Delta G_V + 4 * \pi * r^2 * \sigma \tag{2.2}$$

where

r = radius of the crystallite

ΔG_V = difference in free energy

σ = surface energy of the fluid/crystal interface

This function, which is plotted out schematically in Figure 2.1 has a maximum (ΔG_{cr}) which describes the critical nucleus size (r_{cr}). This marks the size a nucleus within the melt has to reach by endothermal growth before it gets energetically favorable for the crystallite to grow further [15].

With the second type of nucleation, heterogenous nucleation, this barrier can be reduced. Polymer chain segments are able to solidify at impurities within the material, thus creating a

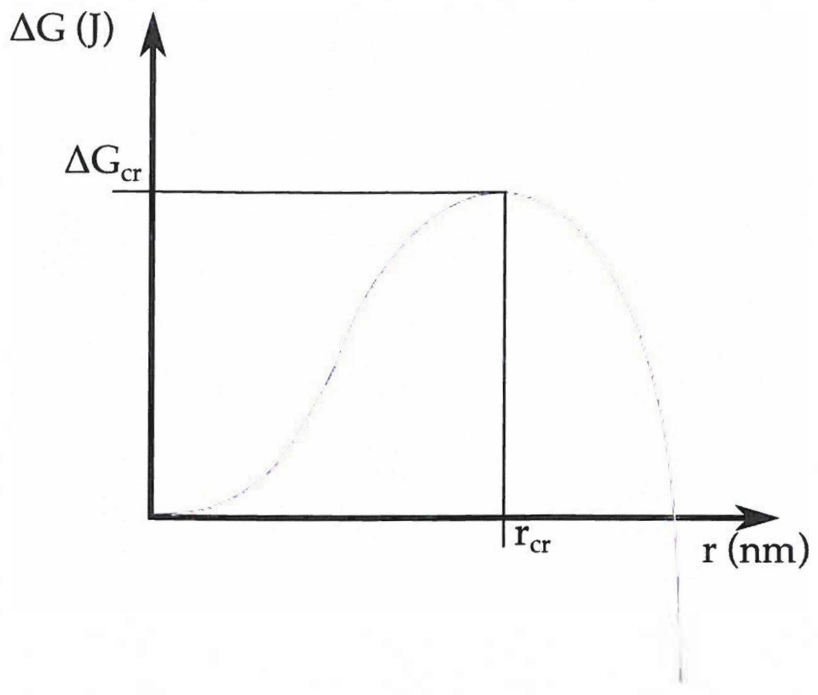

Figure 2.1: Schematic plot of the engery equation of nucleus formation [14].

bigger nucleus to start with and favoring crystal growth. Size and general compatibility of the impurity with the plastic are important factors contributing to the effectiveness of this process [15, 13]. As already mentioned in this section, polymer crystallites are superstructures formed within the same molecule or between different molecules with both cases occuring within the same crystallite. Figure 2.2 shows a crystallite as characterized by the so called solidification model, first proposed by Fischer et al [16]. Here, properly aligned chain segments are incorporated in the crystal (shown as thicker lines), with the uncoordinated segments mostly forming loops and reentering the lamella closely to its exit. Some molecules also can reenter another lamella, thus forming bonds between adjacent crystallites. In this illustration it is also shown that lateral dimensions (X,Y) far exceed the vertical dimension. Going back to Equation 2.2, this is in strong contrast to one of the two main assumptions, namely spherical crystal growth. The second limitation to the applicability of Equation 2.2 being that surface energy at the ends of polymer chains differs significantly from surface energy along the backbone. This leads to a more accurate adoption [12, 15]:

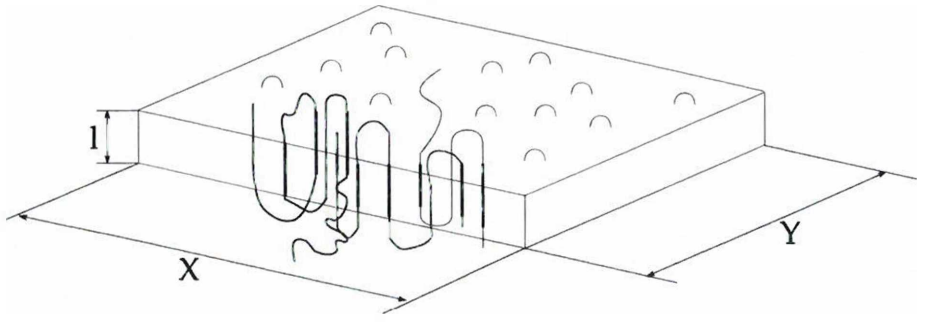

Figure 2.2: Solidifaction model for the crystal phase of bulk crystallized polymers [12].

$$\Delta G_{crystal}(T) = 2 * X * Y * \sigma_e + 2 * l * (X + Y) * \sigma - X * Y * l * \Delta G_v \tag{2.3}$$

With

$$\sigma_e = \text{fold surface free energy} \tag{2.4}$$

This equation leads to the rate of formation I of folded chain nuclei [15, 17]

$$I = I_0 * \exp \frac{-\Delta F_D}{kT} * \exp \frac{32 * \sigma^2 * \sigma_e * (T_m^0)^2}{kT * \Delta T^2 * \Delta H_v} \tag{2.5}$$

With

I_0 = starting rate of formation

ΔF_D = energy barrier for material transport across the melt/crystal interface

ΔH_v = fusion enthalpy per volume

T_m^0 = equilibrium melting temperature of an infinite single molecule crystal

k = Boltzmann constant

These models can describe chain folding nucleation with reasonable accuracy, meaning that only one macromolecule is involved in the nucleus forming process. This is very unlikely the case within polymer melts. Therefore, it is better to assume a nucleus consisting of

aligned segments of different molecules in combination with folded chain segments of these. This means that one macromolecule is able to contribute to numerous crystallites with amphorphous areas between them. This "fringed-micelle" model is first proposed by Flory [18]. While some of the assumptions made are proven to be not applicable, it is still widely used to picture polymeric crystal structures [15]. This model not only incorporates the entropy contribution from melt-crystal separation, but also the limitations of spatial conformation available to the molecules in the amporphous phase, especially to the chain segments adajcent to crystallized segments. Under real conditions however, homogenous nucleation is far outweighed by heterogenous nucleation, thus making it difficult to closely relate nucleation models to experimental findings [15].

2.1.2 Secondary Nucleation

After the first crystals have been formed, it is energetically favorable for further molecules to align themeselves to the edges of existing lamellae. However, the rate at which this process occurs is strongly limited by the agility of the amorphous molecule sections. This agility depends on chain length between crystallized areas, flexibility of the backbone, temperature and more. There is, however, a theory, called "Lauritzen-Hoffmann secondary nucleation theory", which is able to describe this process adequatly. Generally, this theory assumes three states for the chain segments to be incorporated. These are, as depicted in Figure 2.3, the supercooled chain, the activated chain and the attached chain.

At first, the free energy of the polymeric chain adjacent to the existing crystal equals that of the melt, thus being:

$$G_{chain} = G_{melt} \tag{2.6}$$

to transfer to the second state (activated state), the subcooled chain is required to straighten up and create two new crystal surface areas, which marks two losses in entropy. The free energy change for transferring between the two steps is given by:

$$\Delta G_{r,activation} = 2 * b_0 * l * \sigma + \psi * (a_0 * b_0 * l) * \Delta G_r \tag{2.7}$$

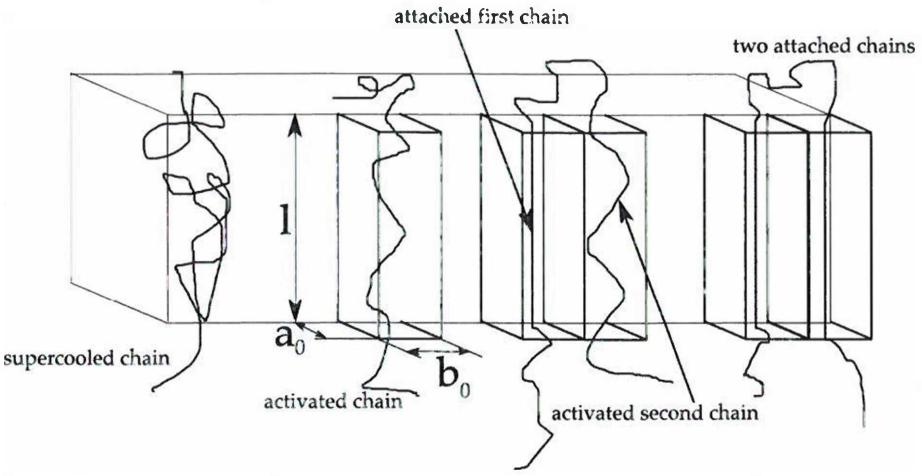

Figure 2.3: The three states of secondary crystallization as stated by Lauritzen et al. [19].

Thus, the free energy of the activated state can be written as:

$$G_{activated} = \psi * G_{crystal} + (1 - \psi) * G_{melt} + 2 * b_0 * \sigma * l \tag{2.8}$$

with

$$\Delta G_r = \text{Gibbs free energy by volume unit}$$

$$\psi = \text{apportionment factor}(\psi + (1 - \psi) = 1)$$

The free energy of the attached chain does no longer include the free energy of the melt, since it is now part of the crystalline phase, therefore it is described by:

$$G_{attached} = G_{crystal} + 2 * b_0 * l * \sigma \tag{2.9}$$

The first term of Equation 2.7 is the energy needed to create the new surfaces, while the second term describes the energy needed for straightening the chain segments. As can be seen from Equation 2.6 to Equation 2.8, the activation step is also the most energy consuming process in secondary nucleation, thus limiting crystallization rate. After the alignment of the first stems, alignments of further chain segments do not produce new surface areas and also reduce total free energy of the growing nucleus until equilibrium is reached. Figure 2.4 shows the amount of free energy needed for the first activation (Step A_0) and for all the subsequent attachments

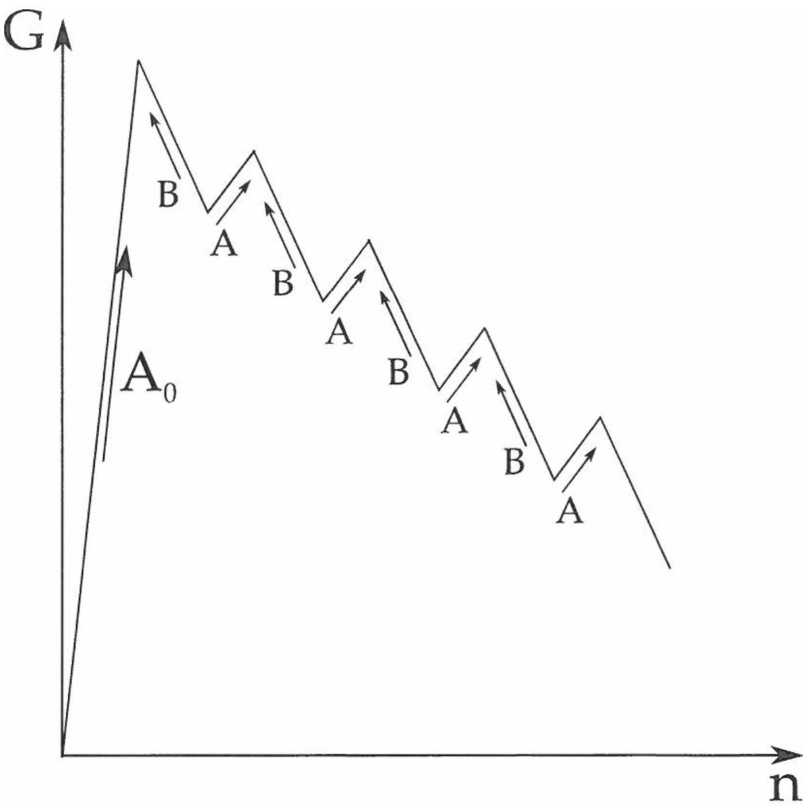

Figure 2.4: Free energy of secondary nucleus formation [19].

(Steps A) over the number of steps n. Also, when free energy is added, the inverse processes (steps B) are also possible [19]. For the nucleus to become stable, it can also be seen that the slope of $\Delta G_{r,activation}$ has to be negative, meaning:

$$0 > 2 * b_0 * l * \sigma + \psi * (a_0 * b_0 * l) * \Delta G_r \tag{2.10}$$

so the critical length a nucleus has to reach to achieve stability can be written as:

$$l > \frac{2 * \sigma}{\Delta G_r} \tag{2.11}$$

2.1.3 Crystal Growth

Within polymer processing, being able to estimate the crystallinity and size of the crystallites is of high importance. Thus, the most important factors influencing the speed of crystal

formation are explained briefly. Most importantly, a high difference in enthalpy between the amorphous state accelerates crystal growth as well as nucleation dramatically. This difference in enthalpy is, as mentioned in subsection 2.1.1, to a great amount caused by supercooling of the melt (the difference between T_m^0 and the temperature of the melt), and helping nuclei to reach critical size. High supercooling also favors the growth of crystallites which are smaller in size, since at every temperature, the formed crystallites are just above their minimum stable size [12, 15]. However, lower temperatures increase melt viscosity, meaning lower chain agility, which hampers the alignment of chain sections. This causes crystallization rate to show a distinct maximum when increasing supercooling. Another factor influencing enthalpy difference is the molecular structure, including constitution and conformation. Linear molecules showing little branching with small and few side groups are able to crystallize far quicker than more complex macromolecules since there are more spatial combinations of unit cells available to form energetically favorable superstructures. Further influences on crystallization rate are flexibility of the polymer chain, average molar mass and molar mass distribution [13].

2.1.4 Spherulites

Large structures consisting of a great number of cristallized molecules possessing up to three dimensional symmetry are found within many different classes of materials. Semi crystalline polymers do also show this kind of arrangement called spherulites. Spherulites can reach dimensions up to 1 mm and most of them show birefringence, making it possible to observe them using polarized light optical microscopy.

Figure 2.5 shows the growth of spherulites radially from the center, where the original nucleus has formed. It can also be seen that ring like structures can occur within the spherulite. This is very likely caused by spiral stacking of the vertical dimensions of the lamellae forming spherulites. When polarized light crosses the crystalline areas parallel to the chain axis of the macromolecules, its polarization angle is not being changed. However, if spherulitic growth only happens in a single plane, this structures are absent. The size of spherulites is dependent on the supercooling during crystallization, thus a high nucleation rate due to a highly supercooled melt leads to smaller, but significantly more spherulites while little supercooling allows

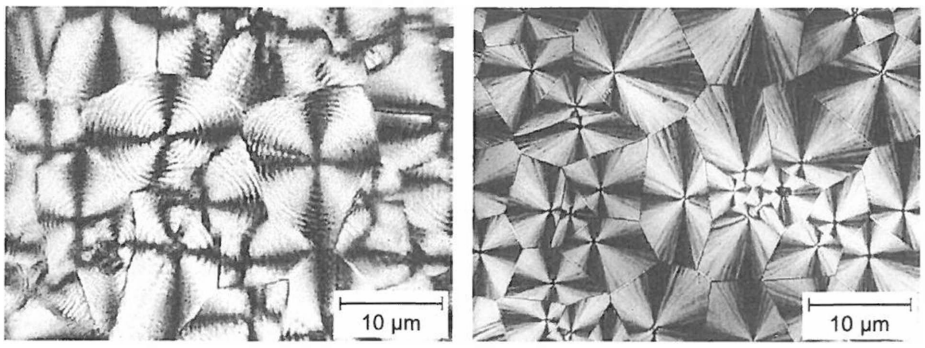

Figure 2.5: Spherulites of crystalline areas of PE as observed using polarized light optical microscopy [20].

the few formed nuclei to grow to bigger spherulites.

There is disagreement as to how spherulite size influences mechanical properties. Some studies suggest that within the material, cracks only grow along the borders between spherulites, thus forcing the crack to take detours, which increases the energy disspation. Other studies, however, clearly show microscopic images of cracks going through spherulites [12, 20, 13].

2.1.5 Epitaxial growth - Shish Kebab

The orientation of macromolecular chains, as briefly mentionend in subsection 2.1.1, can facilitate their transition into a crystalline state. When strain is applied to a polymer, its macromolecular chains rearrange themselves to get aligned in the direction of strain, causing them to leave their entropically favorable amorphous state to go into a state of lower entropy. This also lowers the free energy barrier for the formation of a stable nuclues and increases the crystallization temperature. These linear crystallites offer nucleation sites for molecules in the amorphous state or unoriented chain segments to epitaxially grow folded chain crystallites onto the central stretched chains [21]. This formation, depictured in Figure 2.6 resembles a Shish-Kebab, a popular middle- eastern dish, hence its name.

This structure can increase the mechanical properties of a polymeric material significantly, because load on the streched chains affects their covalent bonds more in line with the direction

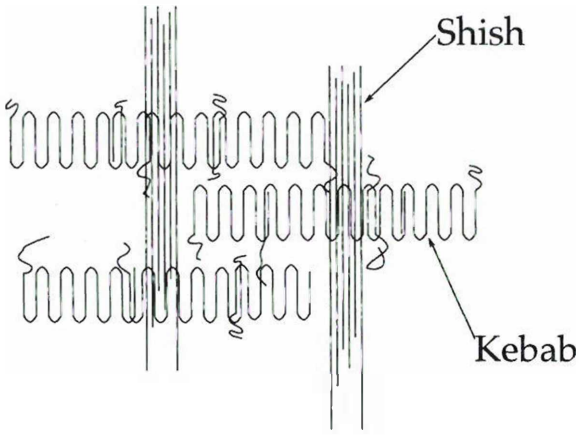

Figure 2.6: Schematics of a Shish-Kebab structure.

of the bond, thus increasing the effect of the binding force. However, a significant increase in Young's Modulus can only be observed with PE, while there has been limited amount of success with PP. It is believed that only in PE, the chains are flexible enough to align at a reasonable amount [20].

2.2 Poly(lactic acid)

In this chapter, the used polymer, PLA is explained further regarding its chemical structure, its crystallization kinetics and mechanical properties. Also, influences of fillers and manufacturing on morphology and physical performance are investigated.

PLA is an aliphatic polyester and as such is a thermoplastic, semi-crystalline material sourced from lactic acid or polyglycol acid. These base materials are produced completely out of renewable resources, like corn, sugar and starch [22].

Figure 2.7 shows the formation process of PLA schematically. For industrial size polymerization of high molecule weight PLA, there are three viable routes. First, and most commonly used is ring opening polymerization (ROP) of the cyclic dilactide of lactic acid. However, since the production of cyclic dilactide does also produce various byproducts, purfication steps like distillation, solvent crystallization or melt crystallization are needed, which increases the price of ROP manufactured PLA [23]. Polycondensation of PLA generally leads to very low

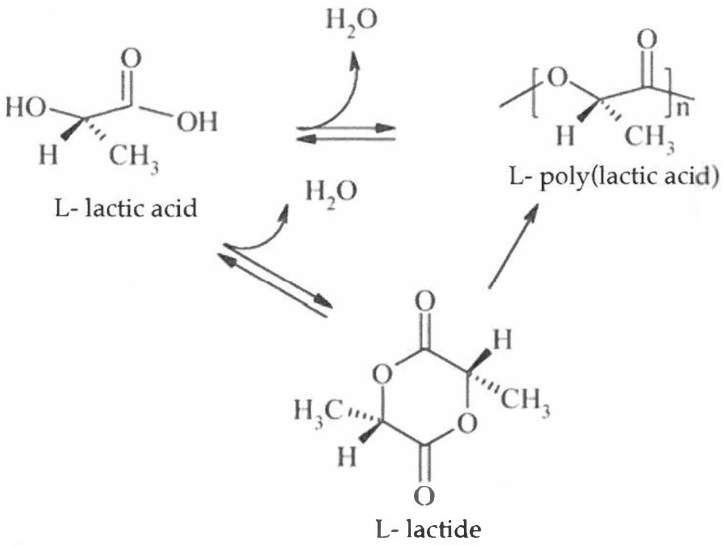

Figure 2.7: Polymerization mechanisms of PLA [22].

molecular weight oligomers, which causes a lot of effort to being put into process management in order to produce higher molecular weight chains. The third approach is to link prepolymers, where, depending on the type of lactic acid the prepolymer is made from, PLA can either show a completely amorphous or semicrystalline structure. Figure 2.8 shows the two enantiomeric configurations of lactic acid. Since the polymer forms ester bonds between repeating units, this chirality is passed on to PLA. It is commonly known that this type of stereoisomerism leads to different light polarization characteristics of chemicals [24]. With polymers however, the effect on steric hindrance of the alignment of macromolecules is far more important. This is also the case with PLA. As mentioned in section 2.2, the compostition of PLA can be controlled via process control. Therefore, three forms of polylactic acid exist: Polymers only containing L or D configurations (PLLA respectively PDLA) and copolymers of PLLA and PDLA called PDLLA . While PLLA and PDLA are semi-crystalline thermoplasts, atactical PDLLA is of amorphous structure [25]. PLA prepolymers can be comprised solely from L or D lactide, making it possible to purposefully control L/D-lacitde ratio [26].

(*S*)-Lactic acid
L-(+)-Lactic acid

(*R*)-Lactic acid
D-(−)-Lactic acid

Figure 2.8: Enantiomers of 2-hydroxypropanoic acid [23].

2.2.1 Stereocomplexity of PLA

One way of forming stereocomplexed PLA is of course preparing a PLLA/PDLA blend. There remains, however, a high chance of crystallites containing either solely PLLA or PLLD but both in a stereocomplexed way.

The second way to induce stereocomplexity into PLA materials is to use PLA copolymer. There exist three possible groups of polymer chain configuration for PLA copolymers, which are depicted in Figure 2.9. The stereocomplex crystal cells can either show some kind of regularity (Only PLLA chains are ajacent to PDLA chains and vice versa) or the enantiomers within the crystallite are distributed statistically. Cartier has shown that the unit cell of the PLLA/PLDA stereocomplex is of triangular shape with PLLA taking a 3_2 and PLDA a 3_1 helical conformation [27]. For the notation of macromolecular helices it is common to write down the number of repeating monomer units (in this case 10) needed to perform the smallest integer number of 360 degree turns (in this case 3). To achieve a high amount of stereocomplex crystallites, it is required to achieve a 1:1 molar ratio of PLLA and PDLA components within the bulk material. When using polymer blends, this can be achieved relatively easily, when using copolymers, a high level of process control is needed. Furthermore, the optical purity (number of D-LA in PLLA and vice versa) has to be well above 75% for the polymer to form stereocomplex crystallites. Stereocomplex crystallites have a higher melting point than the α phase, making it possible to show their presence using Differential Scaling Calorimetry

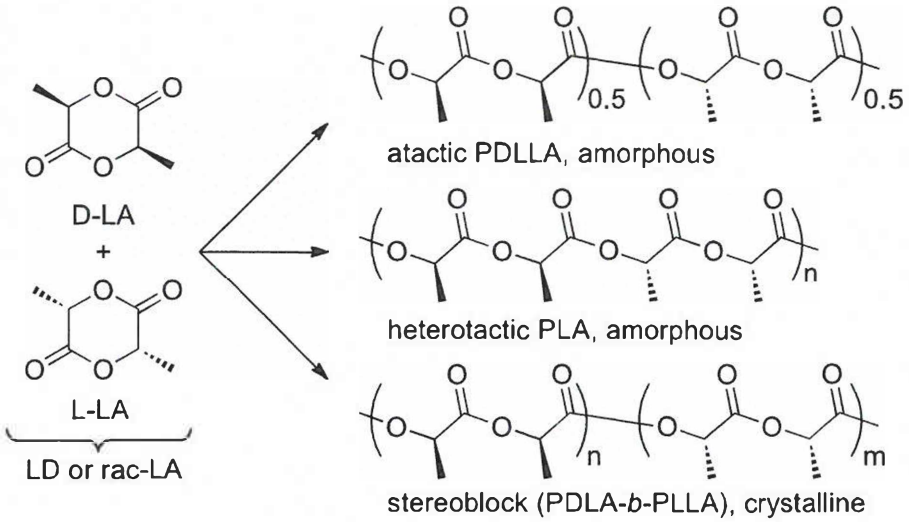

Figure 2.9: Types of PLA configuration created by different enantiomeric compositions of monomers [25].

[25, 28]. Stereocomplexity has important influences on mechanical, rheological and chemical behaviour of PLA. For instance, thermal stability of PLA is greatly increased at temperatures close above T_m, but not at even higher temperatures. It is believed that the strong connection between L and D units lets the helical conformation stay intact even in the melt. But when temperatures rise above a certain level, this bond is also destroyed. Furthermore, it is reported that the resistance to hydrolysis is greatly influenced by the ratio of PLLA/PDLA components of a PLA blend. A 50/50 mixture of both enantiomers can decrease internal energy in the polymer, taking it closer to the low-energy hydrolysed state, thus hydrolyzation is less energetically favorable [23, 28]. Stereocomplex PLA can also be used to a great effect as a nucleating agent in PLLA. Anderson and Hillmyer prepared PLLA/PDLLA blends with a PDLLA content up to 3% and doubled the nucleation efficiency within the PLLA achieved by adding talcum [29].

2.2.2 Crystallinity of PLA

A lot of research has gone into understanding crystal structure and its influences on material properties of PLA. Most of the research done focusses on PLLA with smaller amounts of

PDLA added, since renewable resources mainly produce PLLA [23]. PLA is also subject to crystal polymorphism, with three crystal forms known today. First discovered by De Santis and Kovacs [30] was the α form, which presents itself by two 10_3 helices with antiparallel orientation organized in pseudo-orthorombic, or orthorombic unit cells[31]. An orthorombic unit cell has three main axes: a, b and c, with $a \neq b \neq c$. All angles between those axes are 90 degrees. Figure 2.10 a) shows the first five repeating units of a right winding PLLA helix, while Figure 2.10 shows the orthorombic, base centered unit cell of a PLLA α crystal. The orthorombic base centered structure constists of 2 antiparallel helices. The helices at the edges are all winding in the same direction, and every one of them is also part of three adjacent unit cells, thus contributing only $\frac{1}{4}$ to each unit cell. The center helix, winding in the opposite direction and is only part of this one unit cell, thus being counted as 1 full helix. The melting temperature of PLLA α crystals is reported to be around 185 °C [23]. However, when crystallization peak times of isothermally crystallized samples are plotted against different crystallization temperatures, two significantly distinct regions separated at around 113°C are found [32]. X-ray Diffraction (XRD) investigation showed different refraction intensities of samples crystallized just over and just under 113°C. This is due to the existence of an α' structure, which only slightly differs from the α crystallites and is formed when crystallization occurs at low temperatures [33].

The β form was first discovered by Eling et al. while spinning PLLA fibers from the melt [34]. It has a lower crystal melting point compared to α PLLA of around 171°C, and the β form of PLLA crystals shows almost hexagonal packing [35], with some research suggesting a frustrated structure to accomodate different orientations of adjacent helices. The general idea of frustrated crystal structures is the inability of the material to absolutely minimize the free energy of all its components. For example, the circumstances of β crystallization of PLLA (temperatures below melting, high shear) do not allow for the establishing of areas where all neighbouring helices are parallel. The frustrated structure seeks to minimize free energy between antiparallel helices within one unit cell. This is mainly done by an angular shift in the base plane and a shift along the c-axis of the unit cell. Figure 2.11 shows such a frustrated unit cell. The most prominent methyl group of the helix at the edges faces upwards while

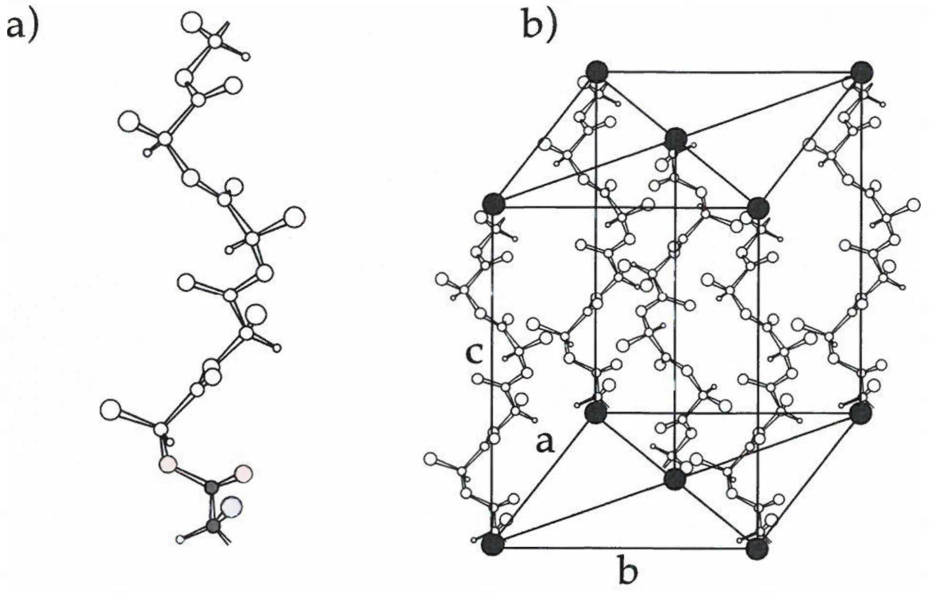

Figure 2.10: a: the first five repeating units of a right winding PLA helix. Color depicting: red=Oxygen, black=Carbon, blue=Hydrogen, purple=methyl group; b: unit cell of α-PLA (modeled after [30]).

the two helices in the center are oriented in the opposite direction. This packing scheme is called North-South-South. A North-West-West arrangement can also be observed, however it is energetically less favorable [36]

As more research went into creating β crystals in PLA, it was found that this can be achieved by applying shear to α PLA with temperatures just below the melting point of the α crystals. While average molar mass and molar mass distribution seem to be influencing the formation of β crystals, the most important aspect is draw rate. At high draw rates, the crystal structure shifts almost fully away from the α structure [35].

Last, the γ structure was found by Cartier et al. by using epitaxial crystallization of PLA films on hexamethylbenzene [37]. They described the structure of the γ phase to consist of an orthorhombic unit cell containing two antiparallel helices. This is the same packaging as the α crystal, however , the spaceing between chains of the two crystal systems differs greatly. The α unit cell measures 1.066 nm along the a- axis and 2.888 nm along the c- axis, while the γ unit cell measures 0.995 nm and 0.880 nm respectively [23].

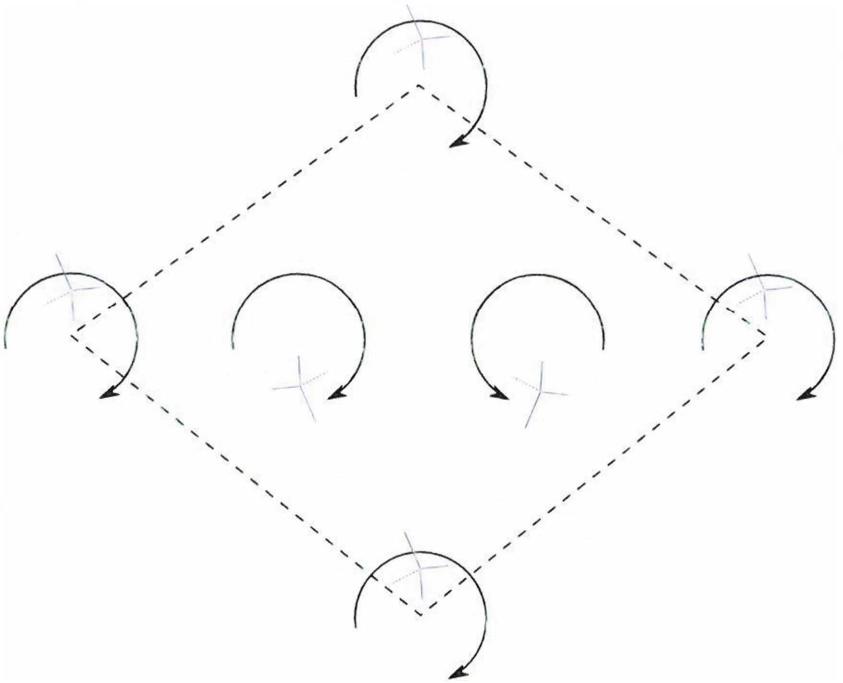

Figure 2.11: C- axis projection of the frustrated structure of β-PLLA, modeled after [30, 36]:

2.3 Modification of PLA properties

With its ability to be sourced only from renewable resources, its good biodegradibility as well as its biocompatibility, PLA, as already discussed in chapter 1, offers properties which become ever more important. However, its widespread use is limited by the often strong temperature degradation of its properties. For example Wang et al. found the Vicat Softening Temperature (VST) of their neat PLA samples to be around 65°C [38]. Furthermore, polylactic acid is prone to degradation during processing and hydrolyzation as well as being pervious to O_2, CO_2 and H_2O [39]. Especially the drop in mechanical properties is often due to the extremely long crystallization times of lean PLA, which far excel typical acceptable cycle times in product manufacturing, with crystallization half time being around 30 minutes at 130°C for unmodified polylactic acid [40]. Therefore, a lot of research has been conducted to improve crystallization behaviour. A very important limiting factor for a more widespread use of PLA for commodity applications is also its relatively high price. This issue can be

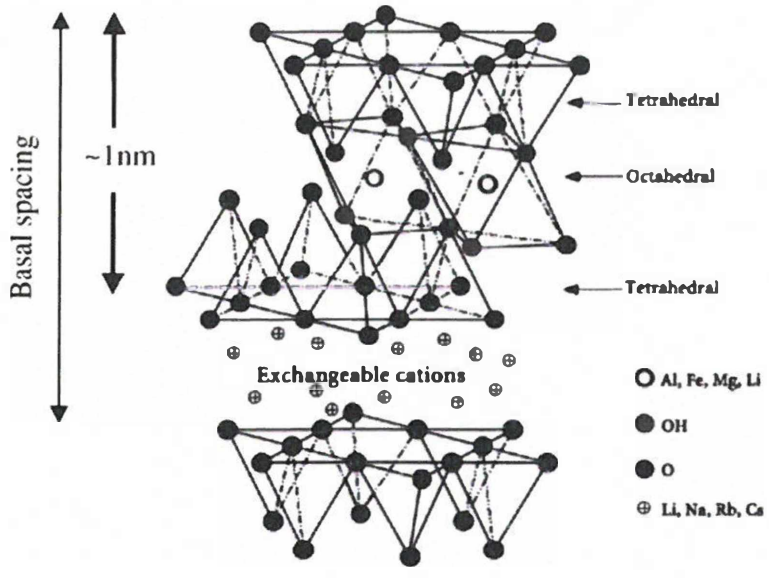

Figure 2.12: Structure of layered silica. [45]

adressed by using cheaper filling materials, which often also affect crystallization kinetics positively. Probably the most widespread filler used across all polymer types is talc, so its influences on the properties of polylactic acid are subject to widespread research. Various DSC and mechanical measurements were carried out over time. All studies showed that talc induces crystallization upon cooling, which is not the case with neat PLA. Also, as talc acts as a strong nucleating agent, it can lower overall degree of crystallinity since the growth of many crystallites slow down molecular rearrangement [41, 42]. However, traditional mineral based fillers render the compound not fully biodegradeable, taking away one of the key advantages of PLA. An also bio-based alternative for talc is starch. Starches have been found to also act as a nucleating agent, decreasing crystallization half time as well as increasing overall degree of crystallinity. This effect occurs already at starch contents as low as 1 %, while the addition of increasing amounts of starch does not reduce the rate of crystallization quite as much [43, 44].

To achieve even higher levels of mechanical and thermal properties, especially under processing conditions, PLA-nanoclay compounds can be taken into account. For polylactic acid, the most commonly used nanoclays are layered silicas like Montmorillonite, Hectorite and Saporite [3]. The basic structure of the silica layers is depicted in Figure 2.12. These hy-

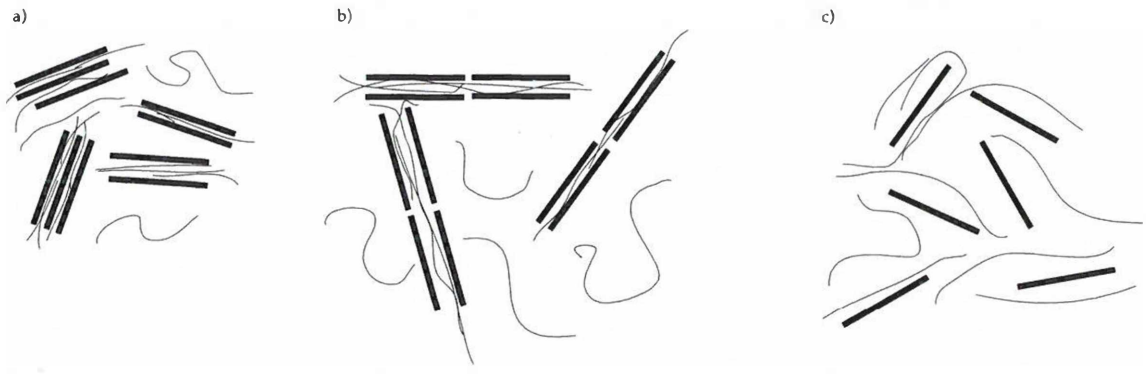

Figure 2.13: Different types of OMLS incorporation into the polymer. a) intercalation b) intercalation with flocculation c) exfoliation

drophilic minerals have to undergo chemical treatment to make them compatible with organic substances. When using these Organically Modified Layered Silicas (OMLS) , the way of incorporation into the polymeric matrix is of great importance to achieve the desired properties. Figure 2.13 shows three different types of incorporation of nano-scale filler materials. Intercalation is characterized by insertion of polymer matrix between layers of filler while still keeping a structured arrangement of layers. Attracting forces between nanolayer edges can cause the intercalated structures to arrange themselves in a flocculated fashion. When single layers of the nanoscale filler are distributed statistically within the polymeric matrix, exfoliation is achieved [46]. Different approaches of preparing nanocompunds have been used over time, from which three should be mentioned. One way is by dissolving a polymer in a solution where the nanoparticles are already exfoliated. This route is convenient for water soluable plastics such as PVA, but organic solvents can also be used to produce polyolefin-nanoclay compounds. While a well exfoliated gel can be achieved until complete drying, sometimes the nanoparticles form agglomerates when the gel is fully dried. Another way of incorporation presents itself by polymerization in the intercalated structure, which is called in-situ intercalative polymerization [47]. The most suitable way to create nanocompounds in the industrial scale is melt intercalation. This can be done without additional chemical substances on readily available equipment such as twin screw corotating extruders. The nanoclay-polymer compatibility is of crucial importance to the success of this method, since it has to be

energetically favorable for the polymer chains to separate the silicate layers [48]. For PLA-nanoclay compounds, intercalation and exfoliation has been achieved using Montmorillonite nanoclay [46, 49, 50, 51]. Many studies find significant increases in Young's Modulus as well as storage modulus of PLA when adding nanoscale materials[39, 47, 2]. This reinforcing effect is especially prominent at temperatures above the glass-transition temperature (T_g) since the nanostructures limit the mobility of the macromolecules [45]. However, to achieve the best effects, good incorporation (intercalation and exfoliation) has to be achieved. When exfoliation is also achieved, the barrier capabilities of PLA can also be greatly improved [52]. To modify barrier properties, another viable way is influencing crystal structure. As mentioned in subsection 2.2.2, when crystallized under quiescent conditions, α and α' crystallites can be formed depending on the crystallization temperature. Due to the slightly lighter packing of the α' crystals, they are significantly more pervious to water vapour. This less dense structure allows for a better ability of the amorphous sections to chanel off strain into crystalline areas, resulting in higher elongations at break [31]. Also, there are other approaches using more specialised nucleating agents, plasticizers or polymer blending to increase material properties of PLA [38, 53, 40].

3 Experimental

3.1 Materials

To investigate nucleation effects in combination with manufacturing conditions, in this work, three different compounds of PLA and filler material were produced in advance. As a base material, Ingeo ™ Biopolymer 3251D (NatureWorks LLC, MN 55345, USA) was used. Table 3.1 shows key physical properties of the plastic as well as the suggested processing conditions by the supplier.

As fillers, two anorganic materials were used. One was pure talc (Finntalc M03 by Mondo Minerals B.V., 1041 AR, The Netherlands), with a top cut (d98%) of 5 μm and a median particle size (d50%) of 1 μm. The second filler material used was Cloisite 20 (Byk Chemie Gmbh, 46483, Germany), an Organically Modified Layered Silica with a median dry particle size (d50%) of 10 μm. It is designed to exfoliate from a micro to a nano scale during compounding. The compounds are composed as shown in Table 3.2.

Since Cloisite is modified with organic portions, the ratio of these were determined using residue on ignition measurements. These measurements were also carried out for Finntalc M03 as a verification, even though no organic portions had to be expected. For these measurements, the filliers were heated at 450 °C in a muffle furnace, with their weight determined before heating and consecutive measurements starting after 3 hours in the furnace. Those measurements were repeated until no further weight loss occured. As expected, no weigth loss occured for talc, while Cloisite lost $28,53 \pm 1\%$ of its original weight. This was taken into account during compounding.

Table 3.1: Key physical and processing properties of Ingeo™ Biopolymer 3251D.

Property	Value	measurement method
Density	1.24 $\frac{g}{cm^3}$	D792
Melt Flow Rate	80 $\frac{g}{10min}$	210 °C, 2.16 kg
Feed Temperature	166-177 °C	proprietary
Compression Temperature	182-193 °C	proprietary
Metering Section	188-205 °C	proprietary
Nozzle	188-205 °C	proprietary
Screw Speed	100-200 rpm	proprietary

3.2 Compounding

Compounding was done using a ZSE27MAXX-440 corotating twin-screw extruder (Leistritz Extrusionstechnik GmbH, 90459 Nürnberg, Germany), which was also outfitted with a vacuum degassing unit as well as an underwater pelletizer. The polymer base material as well as the fillers were fed to the screws using gravimetric scales by Brabender GmbH & Co. KG (47055 Duisburg, Germany). Figure 3.1 shows the screw setup used for compounding, with special markers for sections differing from classical conveying elements. 'S I' depicts the polymer feed section. At the very left, there are double pitch elements which prevent the melt for exiting the compounder at the wrong side. Other elements in the feed section are half pitch for quickly taking material further into the compounder. 'S II' consists of kneading elements for melt homogenization. At 'S III', the fillers are fed, therefore more kneading parts are needed. 'S IV' marks the location of the degassing unit. To lower the pressure in the melt, opposite pitch elements are needed, allowing gasses to dissolve from the melt. 'S V' marks the discharge section, with double pitch elements to ramp up pressure once again. This is needed to overcome pressure loss before the pelletizing unit. This setup was chosen in respect to previous work done at this machine.

Figure 3.1: Screw setup used for processing of the compounds.

Table 3.2: Materials used for Injection Moulding

Material name	Filler content
PLA-N	0 %
PLA-T	5% Finntalc M03
PLA-S	7% Cloisite 20
PLA-TS	2,4% Finntalc M03, 3,6% Cloisite 20

In front of the perforated plate of the pelletizer, a pressure sensor was mounted. This was used for process control. Temperatures of the extruder sections were set to ensure a pressure at this sensor of around 13 bar. The temperature sections of the extruder do not directly correspond to the Sections S I to S V of Figure 3.1, but are evenly spaced across the whole length. Temperatures were set to 165 °C and 170 °C for the first two sections to allow a more gentle melting of the plastic. All following areas were set to 180° C. These temperatures are on the low end of the spectrum given by Table 3.1. This was done in order to damage the material as little as possible during compounding, which could alter the material properties for the injection moulding step. After Compounding, the materials listed in Table 3.2 were further used for injection molding.

As already mentioned, organic elements of Cloisite 20 had to be taken into account when calibrating the gravimetric scales, therefore the percentages given in Table 3.2 were added to the PLA during compounding. The actual calculated percentages were rounded due to the limited precision of the scales as well as to enable easier preparation of the filler for PLA-TS. To ensure a homogenous mixture of the two fillers, they were premixed. In order to do so, a sieve was used to stack thin alternating layers of each filler on top of each other in a container.

After this first stacking, the layered mixture was again sieved into thin layers to insure the homogenous distribution.

3.3 Injection Molding and DOE

For the manufacturing of the samples, a Full-Factorial 3^2 Design of Experiments (DOE) was chosen, because this design allows for good statistical analysis and response surface fitting [54, 55]. Table 3.3 shows the Levels of the two factors annealing time (t_a) and annealing temperature (T_a). When creating the DOE, the design goal was to make it applicable to every material. In order to do so, preliminary DSC measurements were carried out to investigate crystallization temperatures upon cooling of all materials. As can be seen in subsection 4.1.1, peak crystallization happens for PLA-T and PLA-TS at around 110 °C. Also, Battegazzore et al. investigated the heat flow of PLA in the DSC apparatus over time at a isothermal temperature of 110 °C. They showed that at this temperature, adding 5 % talc increases crystallization speed a lot [41]. Kc et al. also investigated crystallization half times of a PLA compound, which contained 1% talc, and found that above 125 °C, crystallization rates were to fast to measure accurately.Thus 100, 110 and 120 °C were chosen as steps for T_a. Crema did investigate crystallization of neat PLA under the same conditions [56]. For the nucleated compounds used in this work, however, a concern was to keep annealing times closer together, because crystallization times should decrease through nucleation [42, 50, 43]. Since there was a risk of not being able to create any noticeable differences between DOE settings for PLA-N, additional specimens were manufactured at $T_a = 900s$ and $t_a = 110C$.

Table 3.3: Design of Experiments.

	t_a /s	T_a /°C
Levels	0 (t1)	100 (T1)
	120 (t2)	110 (T2)
	240 (t3)	120 (T3)
extra setting	900	110

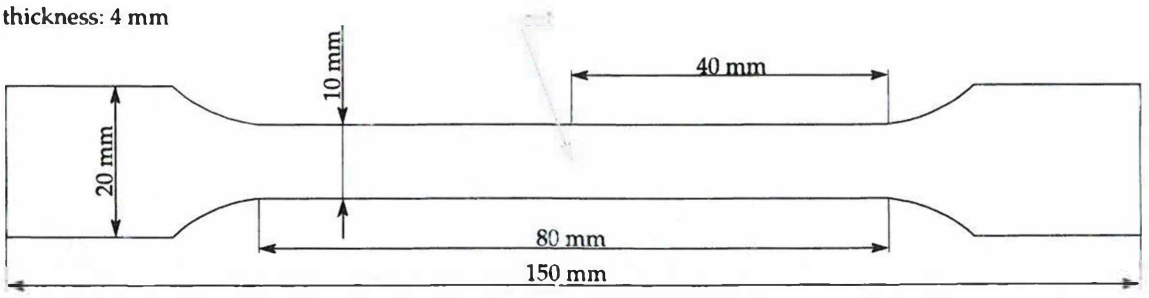

Figure 3.2: Dimensions of a DIN EN ISO 527-1A multipurpose specimen including the position of sample cut outs.

Table 3.4: additional process settings which were not altered during DOE.

mold temperature /°C	clamping force /kN	injection volume flow / $\frac{cm^3}{s}$	packing pressure /bar
30	1100	100	350

This Design of Experiments was carried out using a Battenfeld HM110/130V injection molding machine (Wittmann Kunststoffgeräte Ges.m.b.H., 1220, Austria). This machine has a maximum clamping force of 1100 kN and is ready to be operated with a RHCM process. In order to do so, the mold was also equipped with two ceramic heating pads (Ultramic®, Watlow Electric Manufacturing Company, MO 63146, USA) for RHCM situated in the middle of each cavity, while cooling was carried out on both mold halves by water cooling. It also featured two cavities for producing two identical specimens compliant with DIN EN ISO 527-1A at once by using two film gates. The geometry of those multipurpose specimens is depicted in Figure 3.2. Figure 3.3 (a) shows the inside of the mold used for specimen manufacturing. Figure 3.3 (b) depicts the assembly of the heatingpads in the mold.

During pre-runs using PLA-TS as testing material (due to the fact of containing both fillers), optimal process settings were tried to be found, which would be applicable to all used materials. This applies to all settings including the chronological sequence of all the actions. Alterations to the parameters not part of the DOE were kept to a minimum and only applied in the case of drastic manufacturing problems.

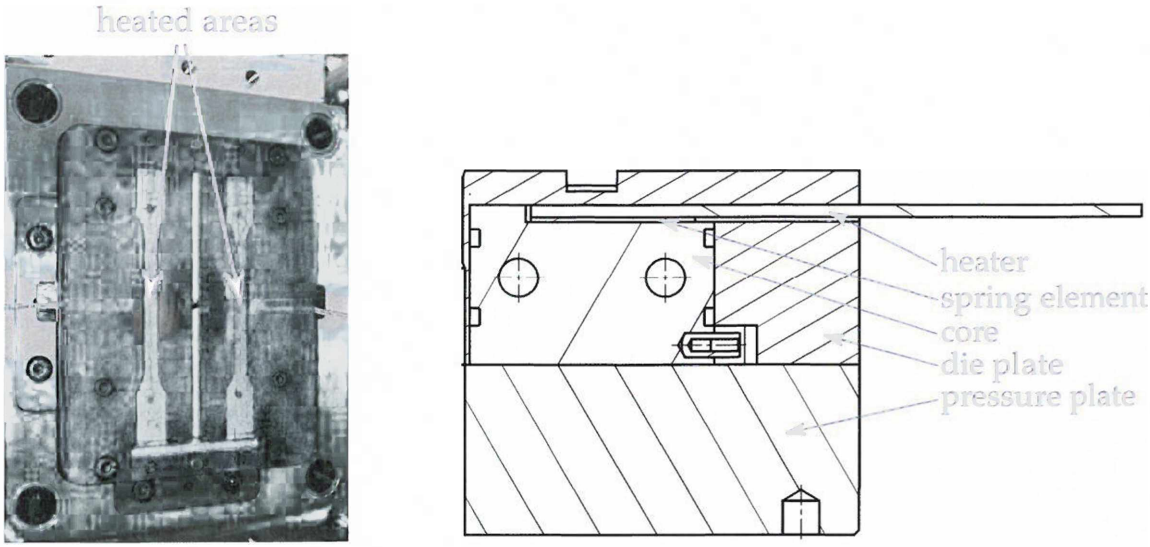

Figure 3.3: Mold used for the injection molding DOE. (a) photo of the cavities, (b) cut through the mold.

Figure 3.4 depicts a whole exemplary cycle of the process used for specimen manufacturing. It mainly depicts the non-varied actions within one cycle. The amount of time left out of the time axis depends on the DOE point Table 3.3. The cycle time without the annealing phase was 79 s for all specimens. From these, 50 s account for the cooling phase after annealing. This had to be done with the mold closed for temperatures to settle back to 30 °C quickly. Also, the demolding process was unstable when it happened at an earlier time. The dosing period took about five seconds, whith the mold opening 8 seconds after the dosing started. Start of injection was 18 s after the cycle start, and packing time was about 20 s, with annealing starting after 10 seconds. This was done to make sure the specimens has already cooled to the no flow temperature at the time the annealing starts. If annealing would start at the same time packing pressure was applied, there would be a high likelihood for the melt not touching the mold surface because of shrinkage, thus, no proof of the effectiveness of annealing during the first few seconds could have been given. Also noticable is the small decompression at the end of the packing phase. In order not to damage the material in the injection unit, dosing happened at the end of the annealing and cooling phases, thus, decompression had to be done

earlier than normal in the injection molding cycle. The screw stroke was 52 mm, however the exact screw positions varied according to the material cushion fluctuations described in subsection 3.3.1.

Table 3.5: Temperature profiles used during injection molding.

	nozzle /°C	cylinder 3 /°C	cylinder 2 /°C	cylinder 1 /°C	feed throat /°C
PLA-N,T,S	195	195	175	155	20
PLA-TS	200	195	185	170	20

Additional process settings which were not altered during the whole manufacturing process are given in Table 3.4. Unfortunately, to make the manufacturing work, some changes had to be done to the temperature profile of the injection unit when switching from PLA-TS to all the other materials. Table 3.5 shows the two temperature profiles used for manufacturing.

3.3.1 Challenges during Injection Molding

As mentioned in section 3.3, injection molding trial runs were conducted using PLA-TS. These trial runs were needed in order to investigate possible problems during manufacturing. PLA-TS was chosen to do the preliminary trial runs with, since it contains both filler types. During these trials, a few key points, where manufacturing problems might occur, have been detected. One, demolding was always challenging. Due to the annealing, the shrinkage around the heated mold areas was less, thus causing the specimens to stick to the cavity walls. To avoid this phenomenon as often as possible, cooling time after annealing was set to 50 s. This worked for most of the manufactured parts, however sometimes they would be bent by the ejectors while remaining in the mold. PLA-S appeared to be more brittle than the other materials and did sometimes shatter when high ejection forces were applied. Those specimens were taken out by hand and thrown away. As an additional precaution, when DOE settings changed, a small amount of separating agent (Hasco Hasenclever GmbH + Co KG, 58513 Germany) was applied to the mold. Another critical point was the feed throat section of the injection molding

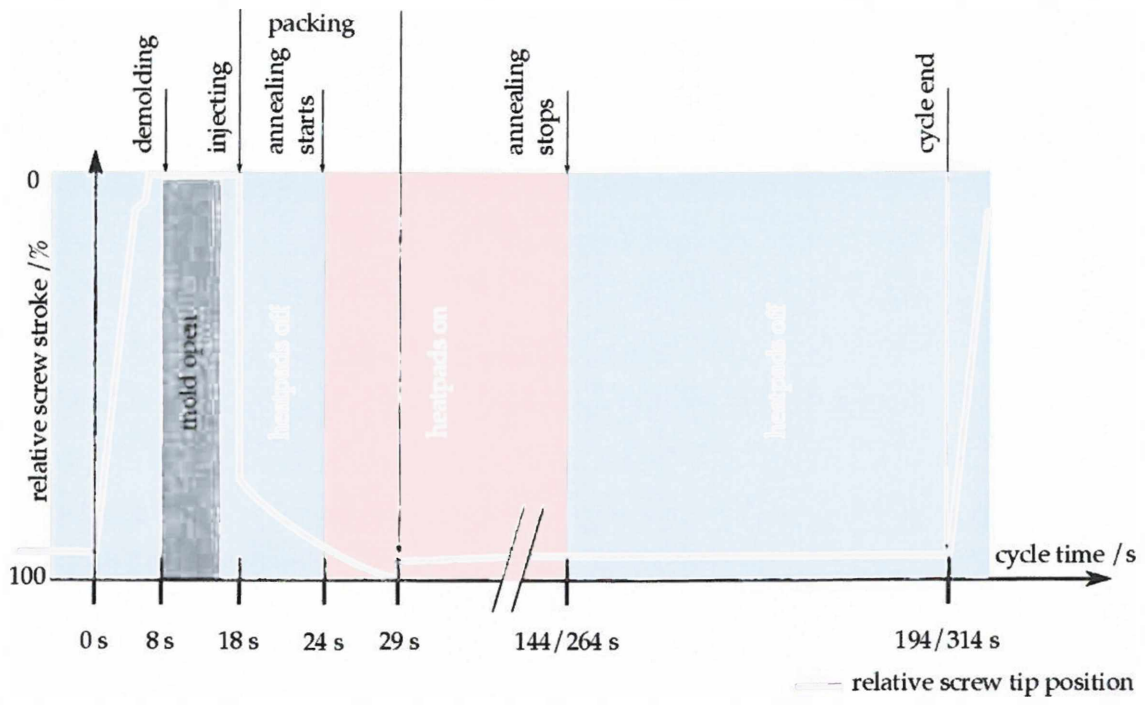

Figure 3.4: Major injection molding process characteristics bound to relative screw stroke during one molding cycle.

machine. This section is actively cooled to be able to keep it at very low temperatures. The compounds had a tendency to stick together even at very low temperatures, thus the feed throat was cooled to 20°C, which is barely achievable with the tethered cooling system. However, at an irregular frequency, agglomerations occured, which lead to fluctuations in feeding speed and dosage.

During the entire DOE manufacturing, significant quality parameters were recorded to investigate anomalies within the process. Those parameters were: Overall cycle time, dosage time, peak injection pressure, material cushion after injection, work used for injection and work used for dosage. Figure 3.5 depicts injection pressure and the remaining material cushion for each shot of the DOE for each material. As already mentioned, the trial runs were conducted using PLA-TS, thus, for this compound, there were no shots with completely dif-

fering pressure values.

There is, however a drift in the material cushion, which is not apparent for PLA-N (a). This drift can be either caused by structural changes of the material, or it is related to the aforementioned feeding problems. To completely rule out material degradation, tests would be needed which were not part of this work. There is, however no evidence of the material deterioriating in the thermal data (like faster crystallization upon cooling), and no such trend can be seen when looking at the quality parameters of PLA-N. What is noticible is that, although no test runs were carried out using PLA-N, the process was extremely stable and no drift in any direction did occur. This also points out that no changes within the neat material were drastic enough to be visible in the quality parameters. Thus, if there were some degradation within the compounds, this could only be caused by polymer-filler interactions. However, no studies on PLA-talc or PLA-silica compounds have noted any accelerated ageing.

Figure 3.5 (a) and (b) do show very unstable material cushions as well as a few shots with very high injection pressures. Specimens of those shots did show significant overmolding, as seen in Figure 3.6, and were not used for further investigations. As already mentioned, the reasons for this behaviour would require much further investigations into the machine state and can be subject to future research.

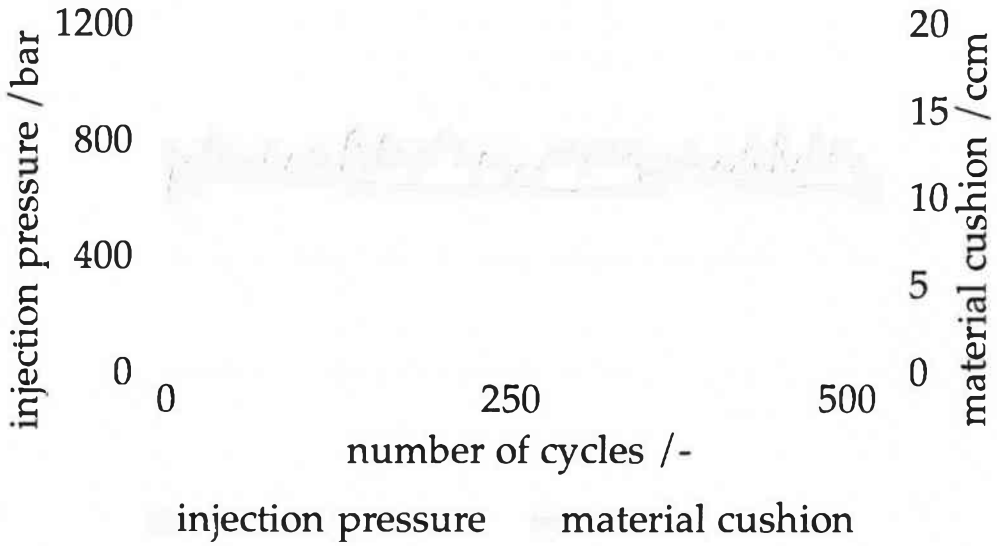

(a)

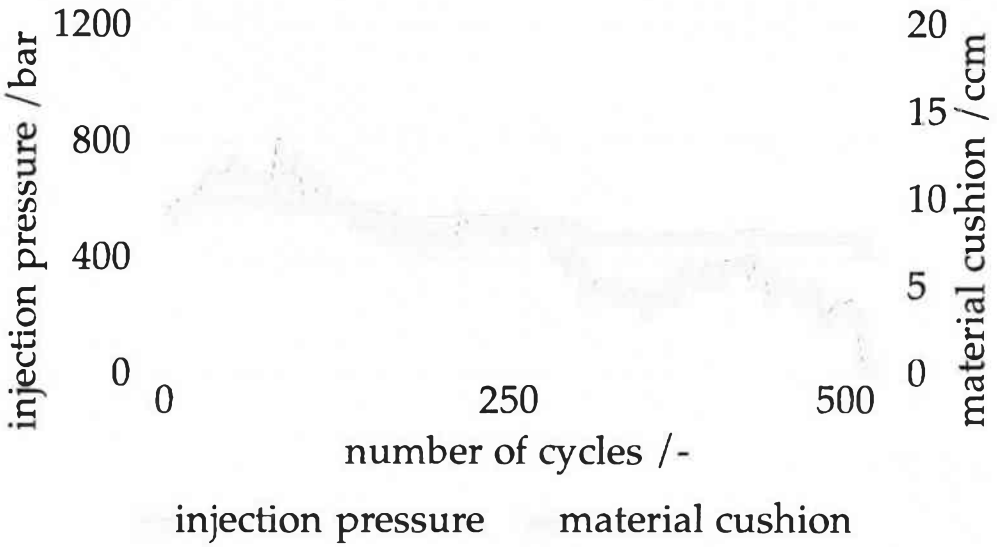

(b)

Figure 3.5: Injection pressure and material cushion as recorded during specimen manufacturing of each compound. (a) PLA-N, (b) PLA-TS

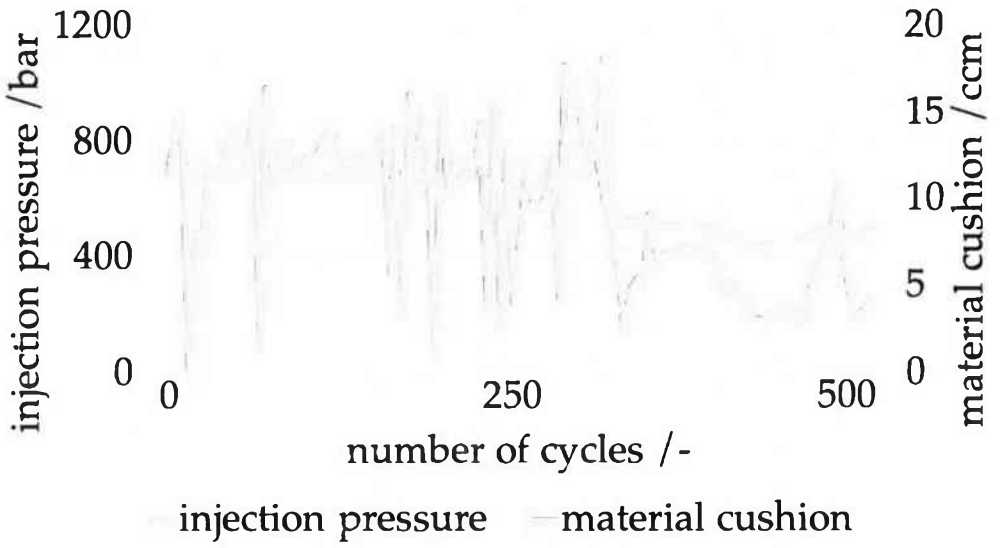

(c)

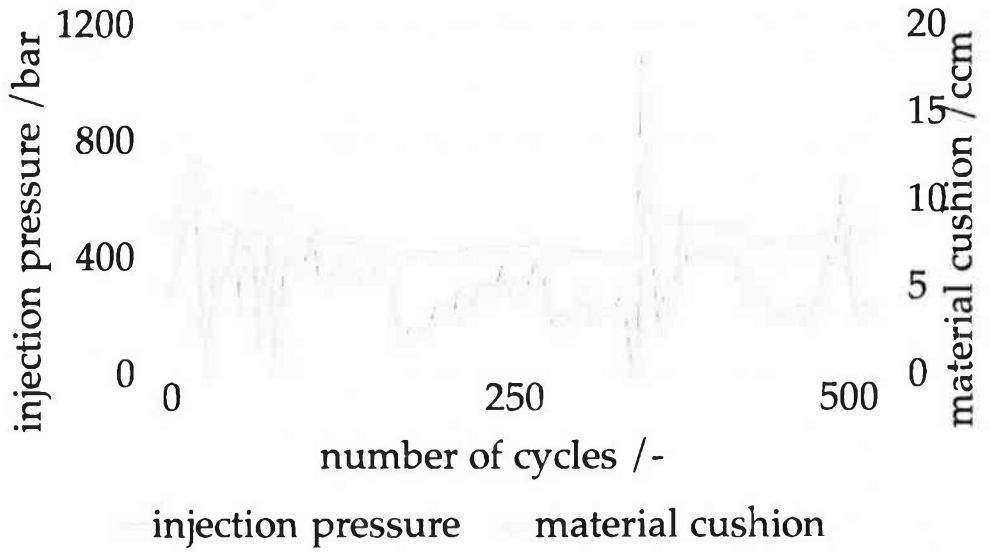

(d)

Figure 3.5: Injection pressure and material cushion as recorded during specimen manufacturing of each compound. (a) PLA-T, (b) PLA-S

Figure 3.6: Overmolded specimen as caused by injection pressure peaks.

3.4 Differential Scanning Calorimetry

The degree of crystallinity, which, in this work acts as the response to the DOE, as well as the melting behaviour of the samples were measured via DSC analysis. The measurements were carried out using a DSC 4000 (by Perkin Elmer Inc, MA 02451, USA). All samples used for this analysis were cut from the multipurpose specimens at the indicated position in Figure 3.2 with a weight of 9,5 $\pm$ 0.5 mg. The measurement program chosen across all types of materials are depicted in Table 3.6. Using this program, the following values were then obtained from the DSC curves: glass transition temperature (first heating run, T_g) enthalpy of cold crystallization (first and second heating run, H_{cc1}, H_{cc2}), melting enthalpy (first and second heating run, ΔHm_1, ΔHm_2) and crystallization enthalpy during cooling (ΔH_c). Thus, the degree of crystallinity (χ) can be obtained using Equation 3.1, with ΔH_{m0} representing the melting enthalpy of the 100% crystalline material (93 J/g for PLA) [41, 57].

$$\chi = \frac{\delta H_m - \delta H_c c}{\delta H_{m0} - (1 - \frac{\%wt\,filler}{100})} * 100 \tag{3.1}$$

Table 3.6: DSC measurement program.

Program Step	Step Characteristics
first heating run	25° C to 240°C at 10° C/min
first hold	240° C for 1 min
cooling run	240° C to 25°C at 10° C/min
second hold	25° C for 1 min
second heating run	25° C to 240°C at 10° C/min
third hold	240° C for 1 min

3.5 Polarized Optical Microscopy

Since the heating pads were only located on the moving mold half of the injection molding machine, a non-homogenous temperature profile was very likely to have been established across the diameter of the specimen. This is done on purpose in order to being able to investigate the heating effectiveness throughout the material. To visualize spherulitic structures within a semicrystalline plastic, a very convenient method is Polarized Optical Microscopy [58]. Also, this method has been used in previous work done on PLA crystallization and is therefore considered suitable for this application [59, 60, 61, 56]. In order to investigate the PLA, samples of the ISO 527-1A specimens had to be prepared. Using a Leica microtome, 15 μm thin slices were cut from the specimens at the same position as the DSC samples. Those slices were then investigated with an Olympus BX51-P optical microscope (by Olympus Corporation, Tokyo, Japan) which was factory equipped with a polarizer as well as an analyzer, a circular polarizer and a top mounted ColorView Soft Imaging System. Pictures were taken using the software analySIS Auto also by the same manufacturer.

3.6 Shore D Hardness Testing

Shore D hardness was tested also at the indicated position in Figure 3.2. This was done using a Test stand 7206.100 (by Zwick GmbH & Co, 89079, Germany). Mounted on this stand

was a Shore D testing gauge compliant with ASTM D2240, DIN 53305 and ISO 868, also manufactured by Zwick GmbH. Testing force was applied for 15 s according to ISO 7619-1, while weights and needles of the apparatus were not adapted to the new standard.

3.7 Thermogravimetric Analysis (TGA)

In order to check the true content of fillers in the PLA matrix after compounding, TGA analysis has been carried out. To do so, a TGA 2 by Mettler-Toledo LLC, OH 43240, USA, was used. 20 $\pm 1 mg$ samples were taken from the pellets of the compounds put into the furnace of the TGA device. The samples were first settled for 10 minutes at 25 °C and afterwards heated to 800 °C at 10 °C per minute. Trial runs were carried out using an air atmosphere in the furnace. However, the PLA burned under this conditions which led to instable sample temperatures. Therefore, a nitrogen atmosphere was used for the measurements.

4 Results

This chapter will display all results gained from DSC Analysis as well as show the polarized optical micrographs and the hardness tests made to establish relationships between measured values and visible morphology of the different compounds.

4.1 Results of the DSC Analysis

DSC analysis is a very powerful tool for material characterization. Its output can give a very thorough insight into the morphology of a material. Therefore, the most important results of the performed DSC scans will be shown here.

4.1.1 DSC Heat Flow Curves

Table 4.1 shows the medium characteristic transition temperatures of the first heating run for all compounds. The values shown were not expected to be influenced by the DOE processing conditions, therefore it is possible to investigate their mean values for each compound [62].

Table 4.1: Characteristic temperatures found in the DSC scans of all four compounds.

Compound	T_g /° C	T_{cc} /°C	T_m /°C
PLA-N	61 ± 1.1	107 ± 1.5	173 ± 0.6
PLA-T	61 ± 1.4	94 ± 0.8	171 ± 0.8
PLA-S	59 ± 0.4	97 ± 1.9	170 ± 0.4
PLA-TS	60 ± 0.4	94 ± 1.1	170 ± 0.4

However, recrystallization temperatures (T_{cc}) for PLA-S are spread out quite high compared to the standard deviations of all other calculated temperatures. This is due to the very distinct shapes of the recristallization peaks of some DSC scans, which could be caused by non- ideal contact areas between the crucibles and the samples. This table also shows the sharply decreased values of T_{cc} and melting peak temperature (T_m). Lower values of these temperatures can indicate nucleation within the material if thermal history and base material is the same for all compared compounds. In this case, all nucleated compounds show this decrease in T_{cc} compared to PLA-N, with PLA-S recrystallizing at a slightly higher temperature than PLA-T and PLA-TS. It hast been shown, that comparing T_{cc} for nucleation analysis is a good indicator for the effectiveness of a nucleating agent [46, 63, 64, 51, 41]. Further insight into the morphology can be gained by comparing overall curve shapes of DSC scans.

Figure 4.1 shows the first heating run of one indicative sample for each DOE setting for each compound respectively. To better visualize the expected differences between the scans, they were separated. Figure 4.1 shows small differences in peak positions, however, this shifts can be due to sample preparation, specifically a non-uniformal contact area of the different samples to the aluminum sample pans [62]. Figure 4.1 (b) to (d) do show a very distinct shape of the melting peak to PLA-N. There is a small exothermic peak right before the start of crystal melting. Yasuniwa et al. and Ke have looked into this for different materials [43, 65]. They state, that for temperatures between the first crystallization peak and the crystal melting, the balance between these two contrary processes can be shifted by nucleating agents. Thus, right before the main melting process happens, increased chain mobility and nucleating agents favor a final recrystallization [63]. Figure 4.1 (b) also shows that there is a noticable drop in recrystallization for all annealed specimens compared to the curve obtained with no annealing. Drops in recrystallization heat flow are however directly connected to the analysis of the degree of crystallinity, thus we looked deeper into this effect in subsection 4.1.2.

Thermal behaviour of the cooling from the melt is shown in Figure 4.2 for all used materials. While as expected, PLA-N did not show any crystallization during these runs, this was also the case with PLA-S, even though some nucleating effect was expected due to previous work and when looking at Table 4.1 [51, 46]. This is very likely caused by an insufficient exfoliation

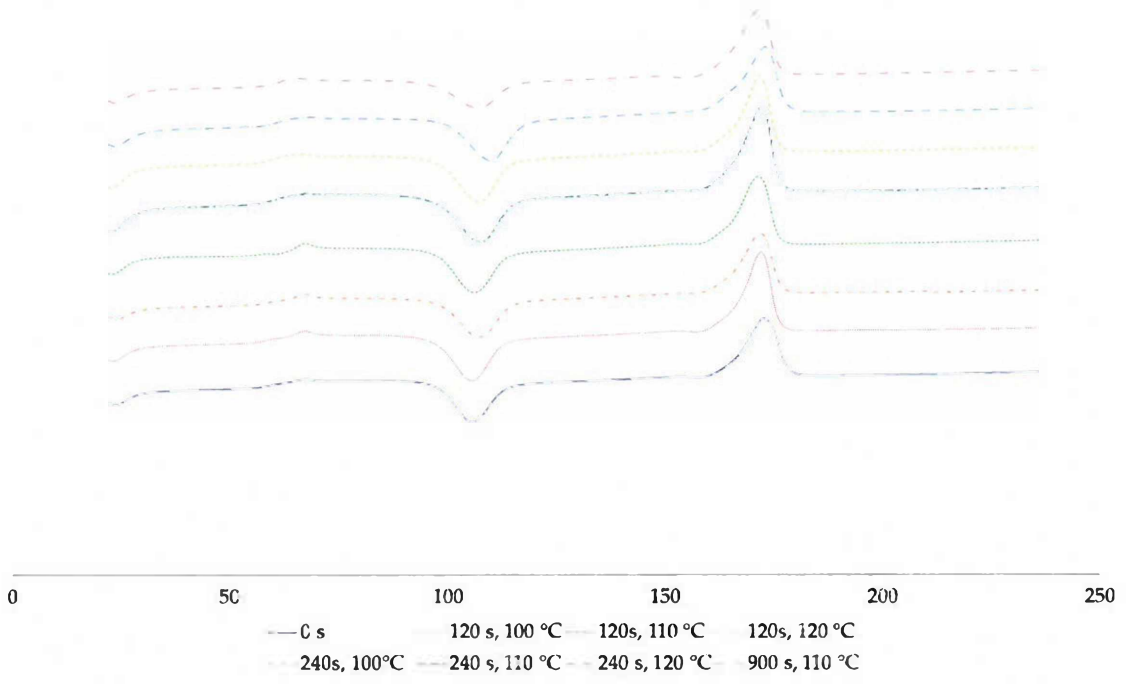

(a)

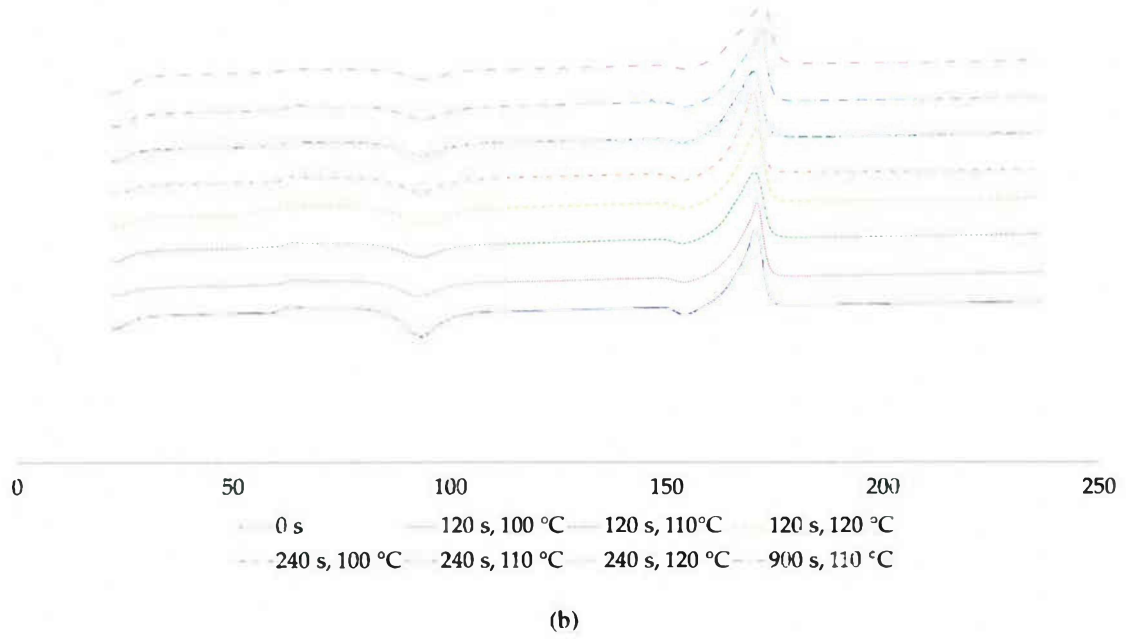

(b)

Figure 4.1: DSC scans of first time heating of the compound samples after manufacturing. (a) PLA-N, (b) PLA-T

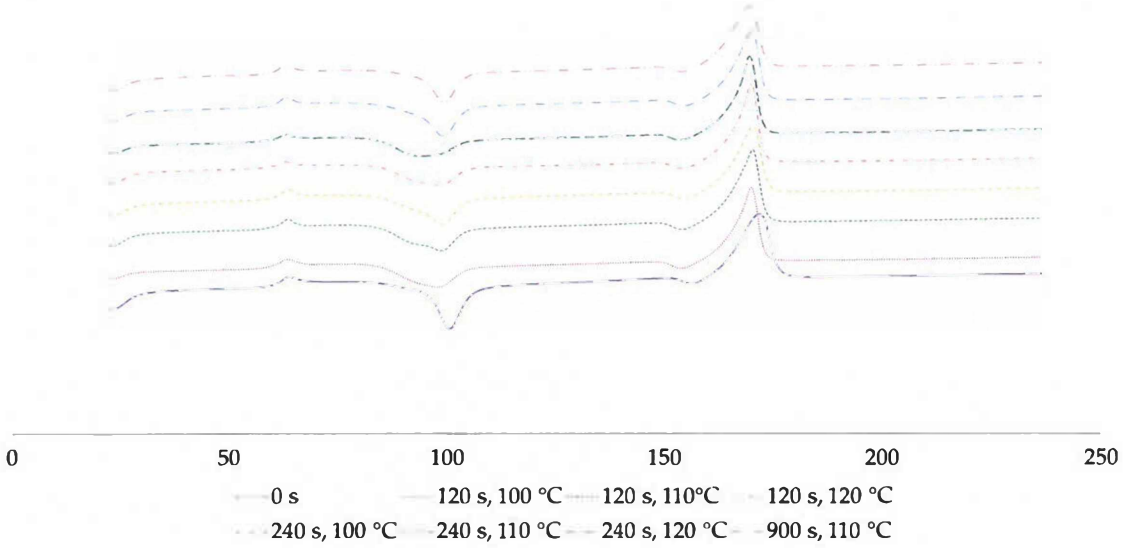

(c)

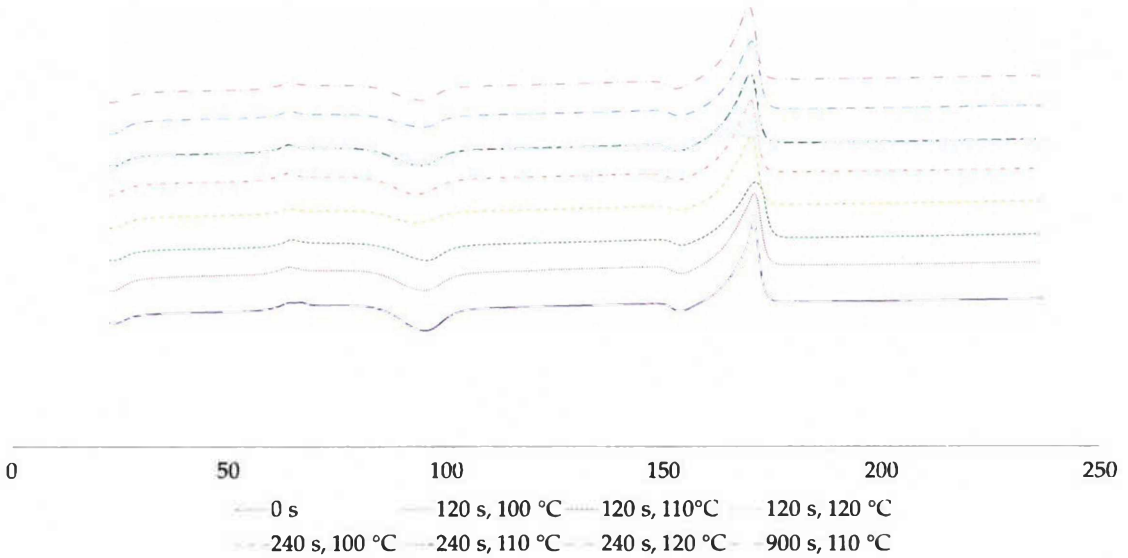

(d)

Figure 4.1: DSC scans of first time heating of the compound samples after manufacturing. (c) PLA-S, (d) PLA-TS

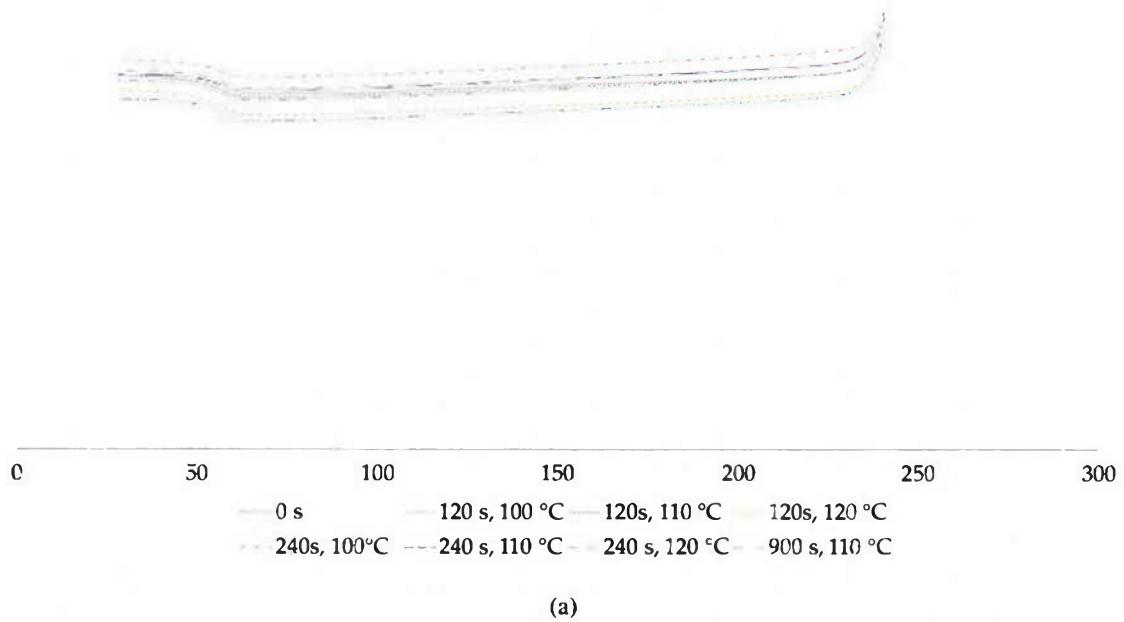

(a)

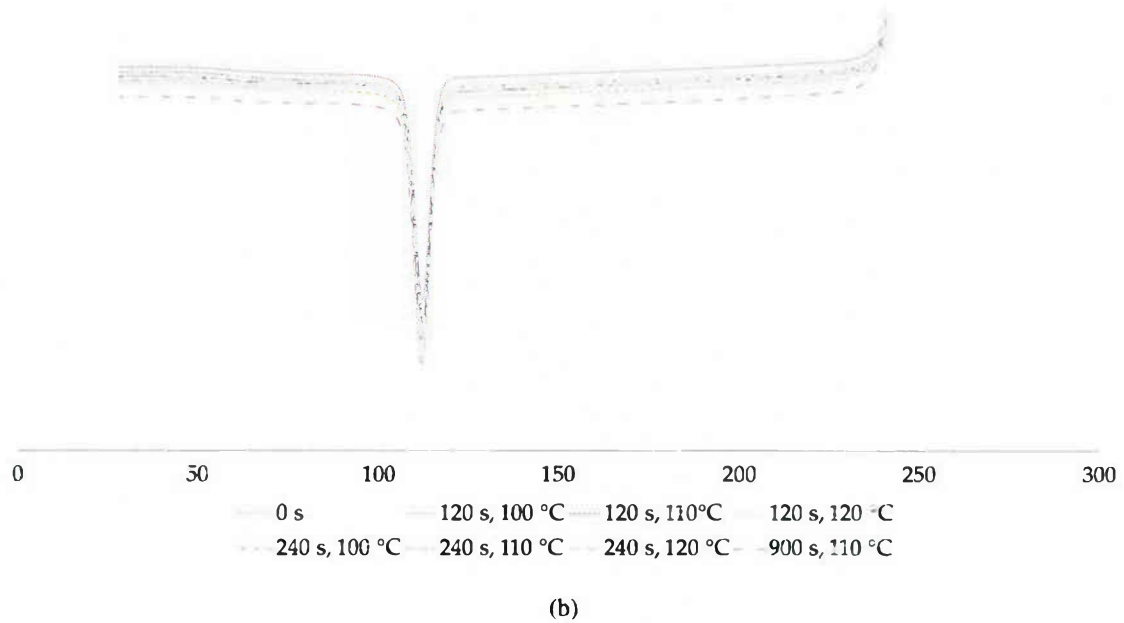

(b)

Figure 4.2: DSC scans of cooling of the compound samples after the first heating scan.

(a) PLA-N, (b) PLA-T

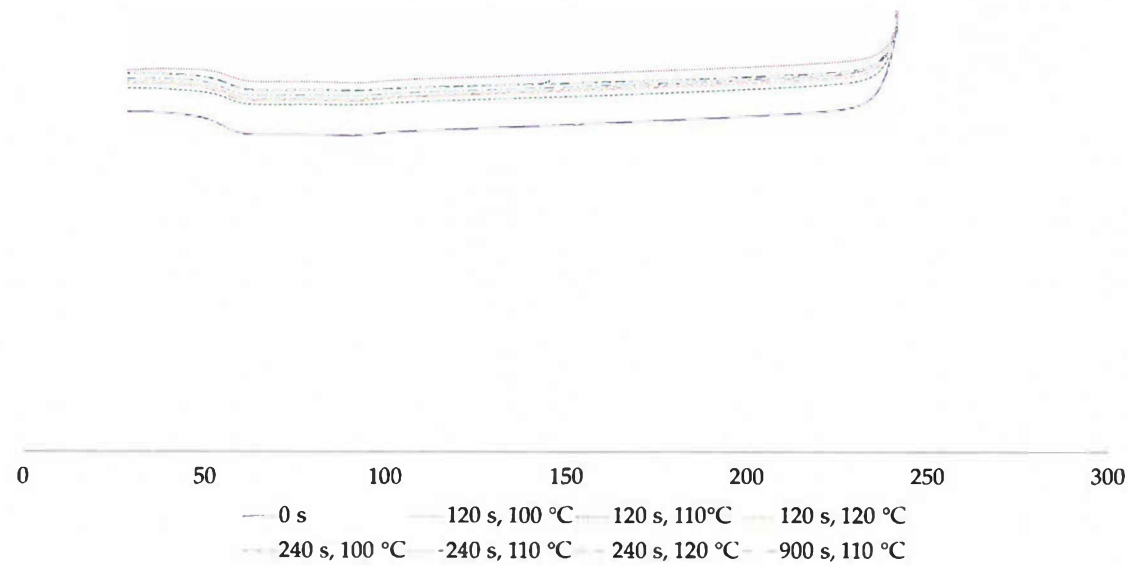

(c)

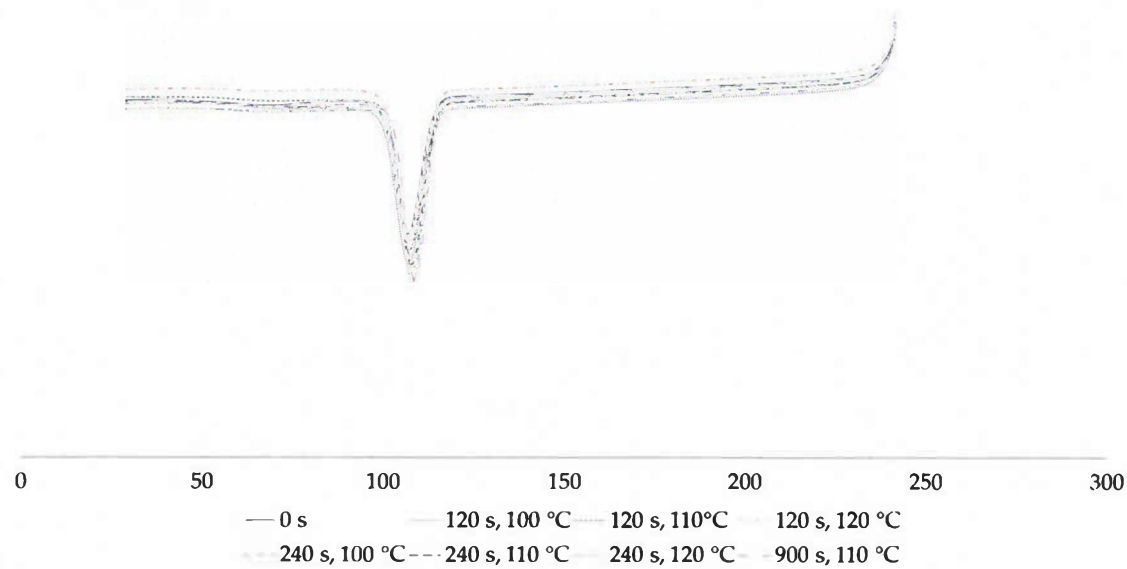

(d)

Figure 4.2: DSC scans of cooling of the compound samples after the first heating scan.
(c) PLA-S, (d) PLA-TS

of the OLMS during compounding [49, 51]. When comparing PLA-T and PLA-TS scans (Figure 4.2 (b) and (d)), crystallization behaviour is as expected. The higher talc content of PLA-T leads to crystallization at slightly higher temperatures ($T_c = 111 \pm 0.5$ °C) compared to PLA-TS ($T_c = 107 \pm 0.5$ °C), which is caused by better nucleation of the compound containing more talc. This can be stated based on the previous made assumption based on Figure 4.2 (c), that the silica has a small nucleating effect. Better nucleation leads to more crystallite formation within a smaller time frame, which causes more crystallites being able to grow to the same size [41]. Size uniformity within the morphology of a material leads to narrower, but higher melting and crystallization peaks in DSC scans [62]. This is visible when comparing average crystallization peak heights of PLA-T and PLA-N which are 1.1 ± 0.08 W/g for the first one respectively 0.8 ± 0.07 W/g for the latter.

The second heating run results are depicted in Figure 4.3. Since thermal history and processing does not influence thermal material behaviour any more, these heating runs are very well suited to investigate general nucleation effects of the different fillers. The data of PLA-N and PLA-S show very pronounced glass transition steps and recrystallization peaks. Recrystallization of PLA-S reaches its peak (102 ± 0.5 °C) earlier than PLA-N (109 ± 1.5 °C) and the peak is also higher (0.7 ± 0.06 W/g to 0.6 ± 0.06 W/g) and narrower. During second heating, the silica acts as a nucleating agent, however to a much smaller extent than talc does.

The compounds containing talc (PLA-T and PLA-TS) do show a completely different thermal behaviour when heated a second time. While crystallization during cooling can pass almost completely with no accurately discernible glass transition and basically no recrystallization, there are two seperate crystal melting peaks. This double melting characteristic has also been found in previous work done with talc filled PLA [42, 63, 64]. The first peak for PLA-T is located at 165 ± 0.35 °C , while the second one is found at 171 ± 0.31 °C. For PLA-T, every one of the two peaks can be the higher one at random samples, while for PLA-TS, the second peak is always higher. Yasuniwa et al. have investigated this phenomenon more closely and stated, that the second peak is the melting peak of crystallites, which have recrystallized at the temperatures of the first melting peak, where the crystals formed during cooling remelted [65].

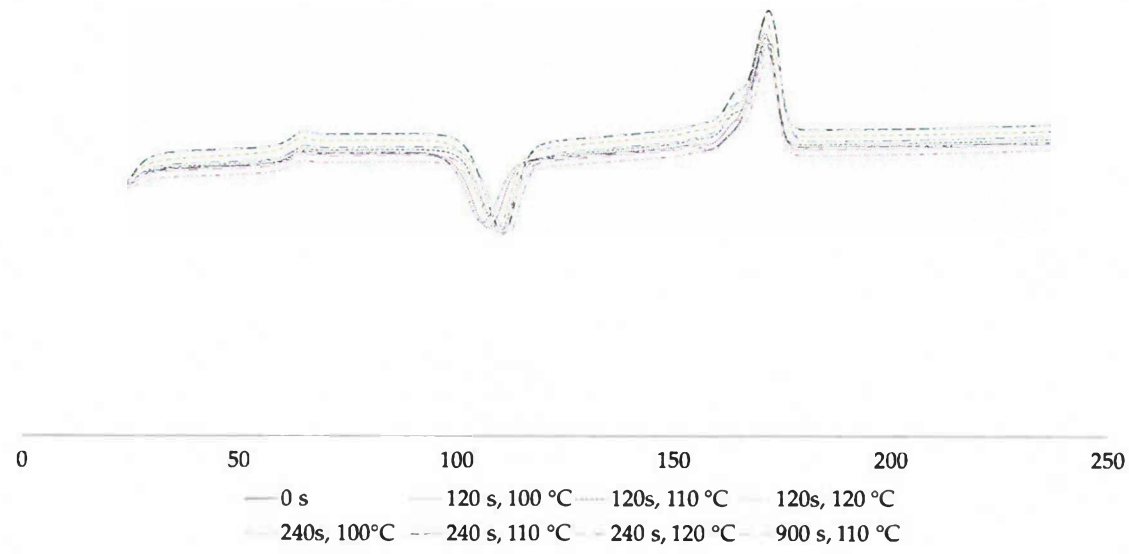

(a)

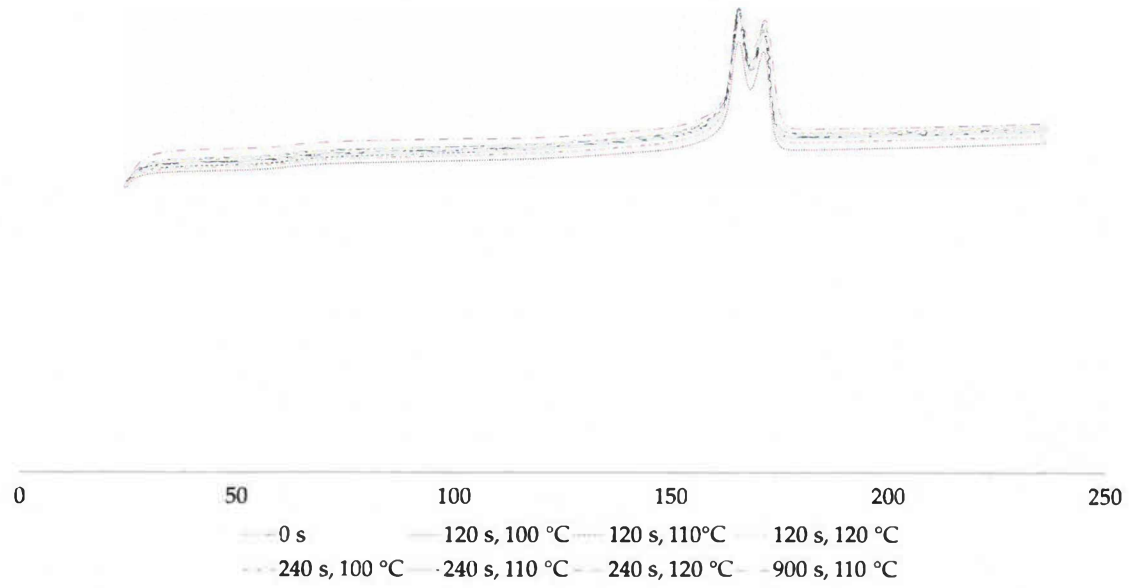

(b)

Figure 4.3: Second heating scan of the compound samples. (a) PLA-N, (b) PLA-T

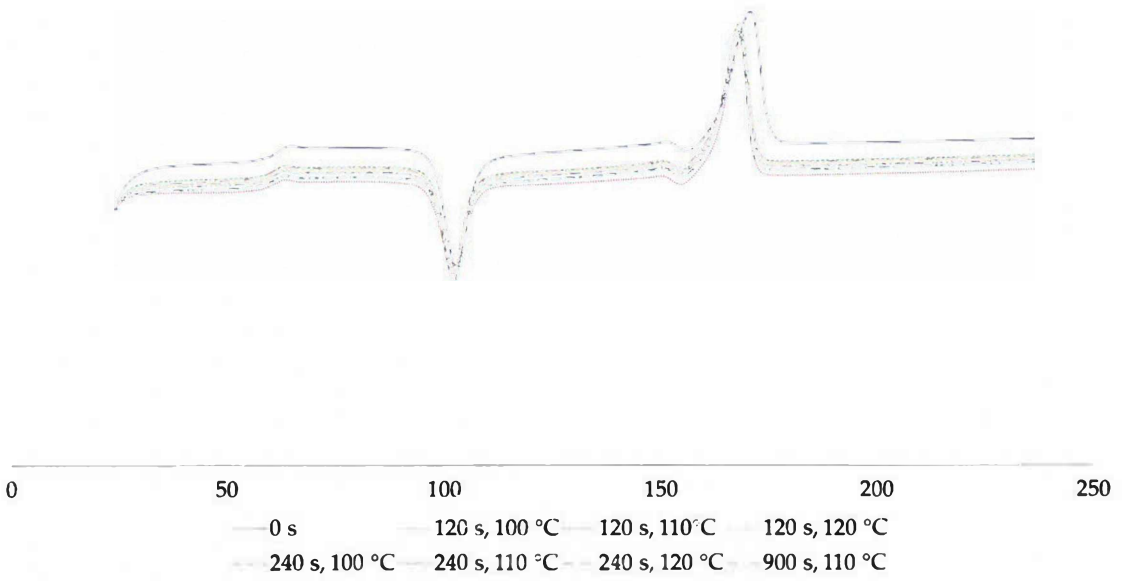

(c)

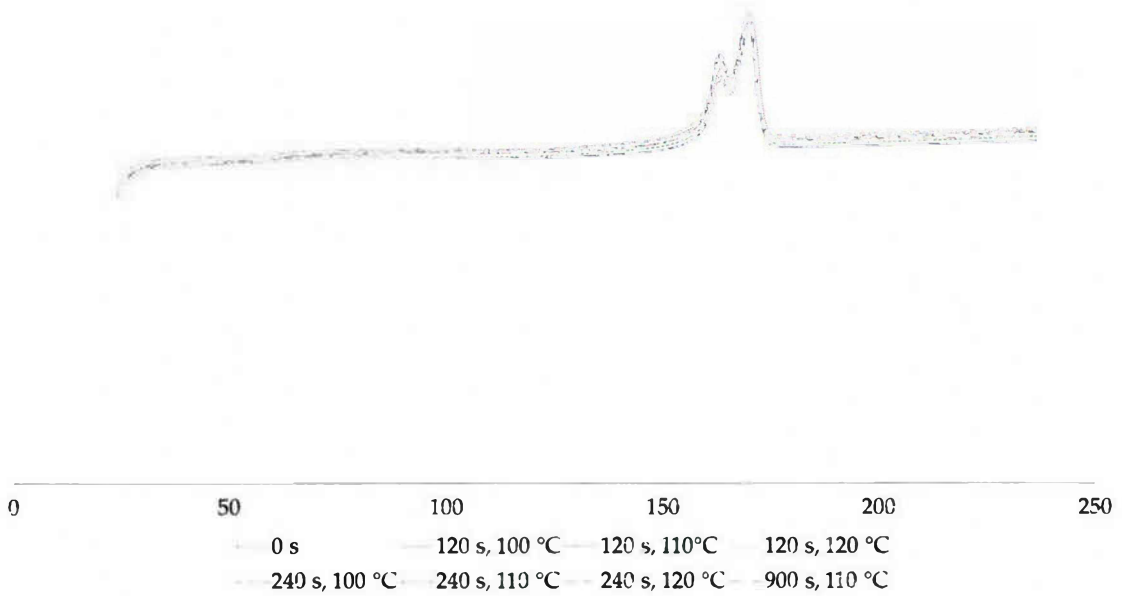

(d)

Figure 4.3: Second heating scan of the compound samples. (c) PLA-S, (d) PLA-TS

While crystal polymorphism has been mentioned in subsection 2.2.2, and is of course visible in DSC scans in the form of multiple melting peaks, in this case, this is unlikely. As mentioned, the α conformation has a melting temperature of around 185 °C, while the β conformation melts at 171 °C [23, 35]. In this work, all melting temperatures are lower, so this would not rule out polymorphism. However, β crystals have only been found when cooling PLA under strain, which is not present in the DSC apparatus [34]. Furthermore, Yasuniwa have found almost the same peaks at temperatures close to the ones found in this work, thus, there is a strong implication for the recrystallization approach [63]. However, to clarify this, more resarch into crystal structure would be necessary, which is not subject to this investigation.

4.1.2 Statistical Analysis of the DOE

To properly evaluate the 3^2 full factorial DOE, which was conducted for every compound, appropriate models were fit to the degrees of crystallinity obtained via DSC analysis using MATLAB (The MathWorks, Inc.). To do so, preliminarily, a full quadratic surface model was fitted to the data via a least squares fitting algorithm, which is readily available in the Software as a pre packaged application. This application allows for the definition of custom equations to be fitted to the data. The quadratic polynomial model used is described by Equation 4.1

$$\chi = a + b * T_a^2 + c * t_a^2 + d * T_a * t + e * T_a + f * t_a \tag{4.1}$$

with

$$\chi = \text{Degree of Crystallinity}$$
$$T_a = \text{annealing Temperature}$$
$$t_a = \text{annealing Time}$$
$$a, b, \ldots f = \text{Coefficients}$$

The fit application returns various goodness-of-fit statistics, such as the root mean square of errors or the coefficient of determination, R^2. The R^2 describes how well the fitted model

Table 4.2: Quality of the first surface fitting run.

Compound	adjusted R^2	probably superfluous coefficients
PLA-N	-0.0870	b,c,d,e,f
PLA-T	0.6517	a,d
PLA-S	0,4062	c,d
PLA-TS	0,9001	c,f

Table 4.3: Best fit model for each compound and their respective coefficients of determination.

Compound	Model	adjusted R^2
PLA-N	$\chi = a + b*T_a^2 + c*t_a^2 + d*T_a*t + e*T_a + f*t_a$	-0.09
PLA-T	$\chi = b*T_a^2 + c*t_a^2 + e*T_a + f*t_a$	0.75
PLA-S	$\chi = a + b*T_a^2 + e*T_a + f*t_a$	0.53
PLA-TS	$\chi = a + b*T_a^2 + d*T_a*t + e*T_a$	0.89

approximates the data points on a scale of 0 (no approximation) to 1 (100% accurate). However, it does not take into account the number of independent variables or the complexity of the fit. Since it is possible to increase the coefficient of determination by fitting higher level polynomials, but totally disregarding the true correlation between the data points, the adjusted R^2 was taken into account for evaluating the goodness of fit. This adjusted value takes into account the complexity of the fit, hence favouring lower level polynomials. Also, for all used coefficients, 95% confidence bounds are given by the software, which helps to indicate the ones who have a high chance of being zero. Table 4.2 shows the achieved adjusted R^2 values of the fits as well as the coefficients which are likely to be zero and thus are being left out stepwise during further fitting cycles. By doing so, the adjusted R^2 was maximised and all remaining coefficients are distinctively different from zero. All non-zero coefficients indicate which of the two factors (T_a and t_a) influence the result and to which degree.

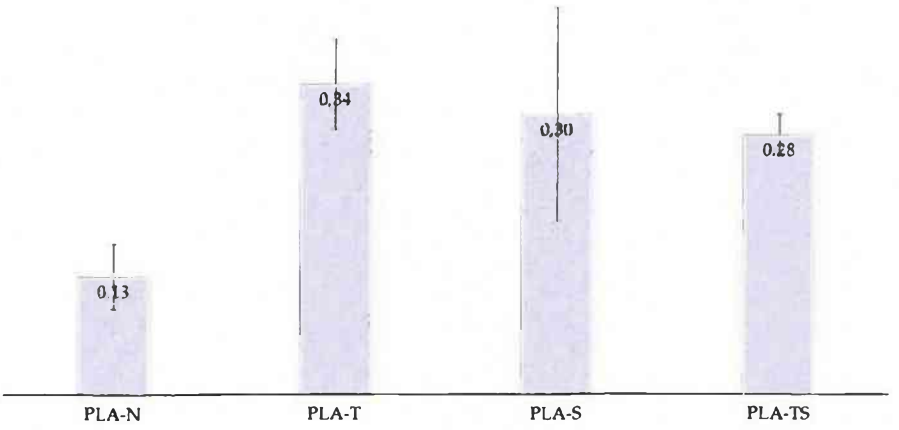

Figure 4.4: Average measured degree of crystallinity (via DSC analysis) of all materials for the control step at 110 °C with 900 s of annealing.

Table 4.3 shows the final fit models for each compound and their respective coefficients of determination. For all compounds except for PLA-TS, the adjusted R^2 values are very low. These results will be discussed in chapter 5, especially in regard to the polarized optical micrographs. Crystallinity of the additional step T2t4 was also calculated and is shown in Figure 4.4.

4.2 Polarized Optical Micrographs

The polarized optical micrographs were carried out for a number of DOE settings, which are best suited to show the effects of the different fillers as well as the process conditions. Furthermore, the inhomogenous distribution occuring due to the heat load only being applied in one mold half, can also be seen in Figure 4.5 to Figure 4.8. They show 10 times magnified images of specimens for the DOE points T1t1, T1t2, T1t3, T3t2 and T3t3 for each used material. All images are aligned to show the edge of the heated side on the left side of each picture, and the border of the sample is indicated by a white marker. To make smaller morphological features more visible, 50 times magnified micrographs were also made for the same DOE settings of PLA-T and PLA-TS. These are depicted in Figure 4.9 and Figure 4.10.

In Figure 4.5, PLA-N spherulites of increasing size can be seen in the images (c) - (d). However, their number remains very small and the highly crystalline border areas in image (d) and (e) remain very thin.

Figure 4.6 shows a very different morphology of the PLA-T compound processed under the same conditions as PLA-N. While the number of spherulites is very high, their size renders it difficult to distinguish them from each other in the 10 times magnified micrographs.

PLA-S, as depicted in Figure 4.7, shows a very distinct white area at the border to the surface in image (b) and (d). In image (c) and (e), likely due to the longer annealing times, this border area has grown to cover the whole micrograph. Their existance is linked to the layered silica, as PLA-N and PLA-T samples do not show them, but their morphology could only be established via further analysis.

Figure 4.8 shows micrographs of PLA-TS samples. As expected, this compound shows features both induced by the talc as well as the layered silica filler material. In image (a) to (c), very fine spherulites are visible similar to Figure 4.6, and image (d) and (e) show the white border area witnessed in Figure 4.7

In Figure 4.9, the 50 times magnification helps to see spherulites in images (a) to (e), even though they appear still very small. This indicates a good nucleation effect by the talc filler.

Figure 4.10 also better shows the smaller talc-induced spherulites in images (a) to (c), however, in images (d) to (e), they are obscured by the white border area already seen in Figure 4.8.

Figure 4.11 highlights the differences in morphology of all investigated materials after 900 s of annealing at 110 °C. It can be seen that PLA-N (a) has formed many large spherulites, but they remain very small and are still hardly visible in PLA-T (b). The already discussed white border area, which PLA-S (c) established, grew extremely brittle, thus making it impossible to prepare clean samples of this compound. PLA-TS (d) again shows, as expected, features of both compounds PLA-T and PLA-S. The micrograph of PLA-TS shows a smaller, less brittle border area than the one seen in image (c) and spherulites which are bigger and better visible than the ones in image (b).

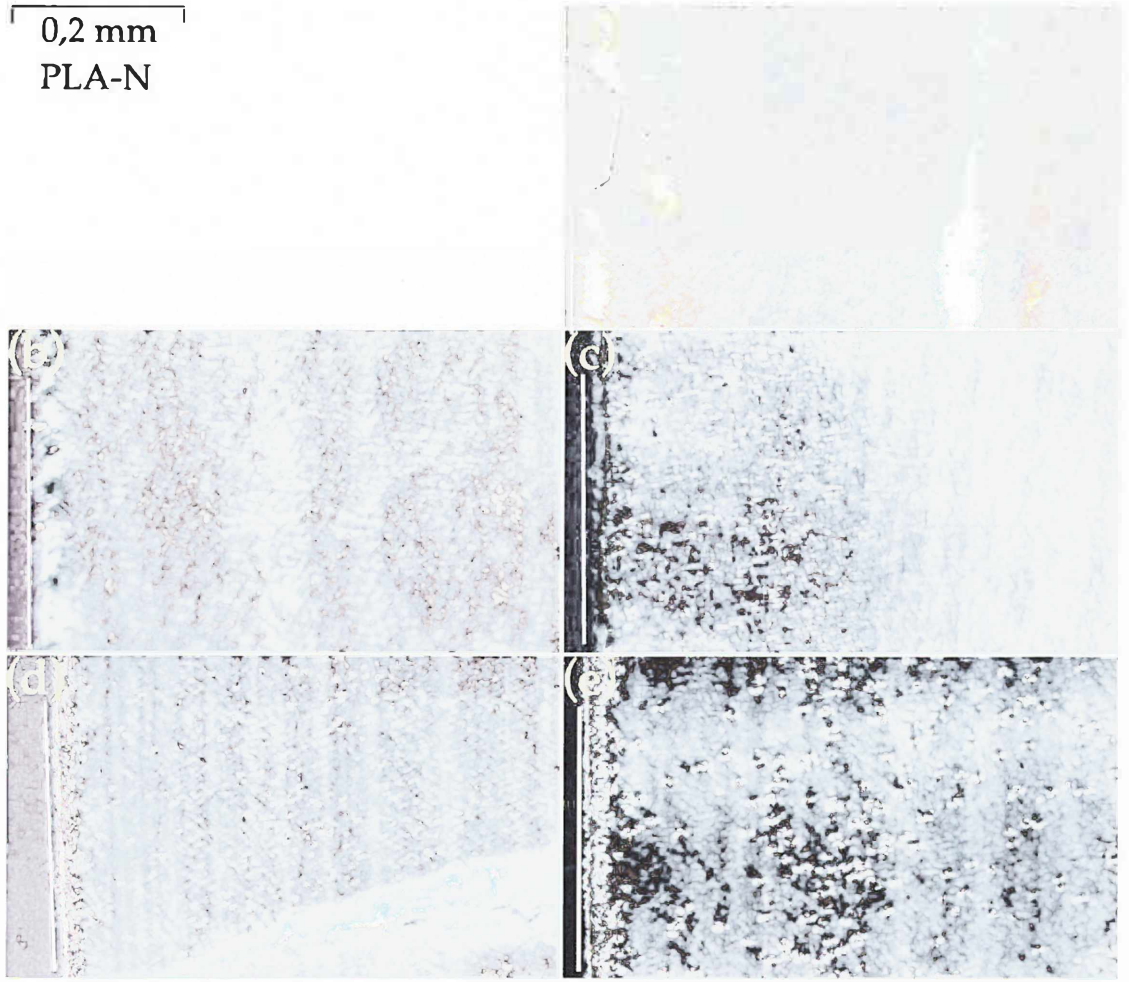

Figure 4.5: Ten times magnified polarized optical micrographs of PLA-N for selected DOE points (a) T1t1, (b) T1t2, (c) T1t3, (d) T3t2, (e) T3t3.

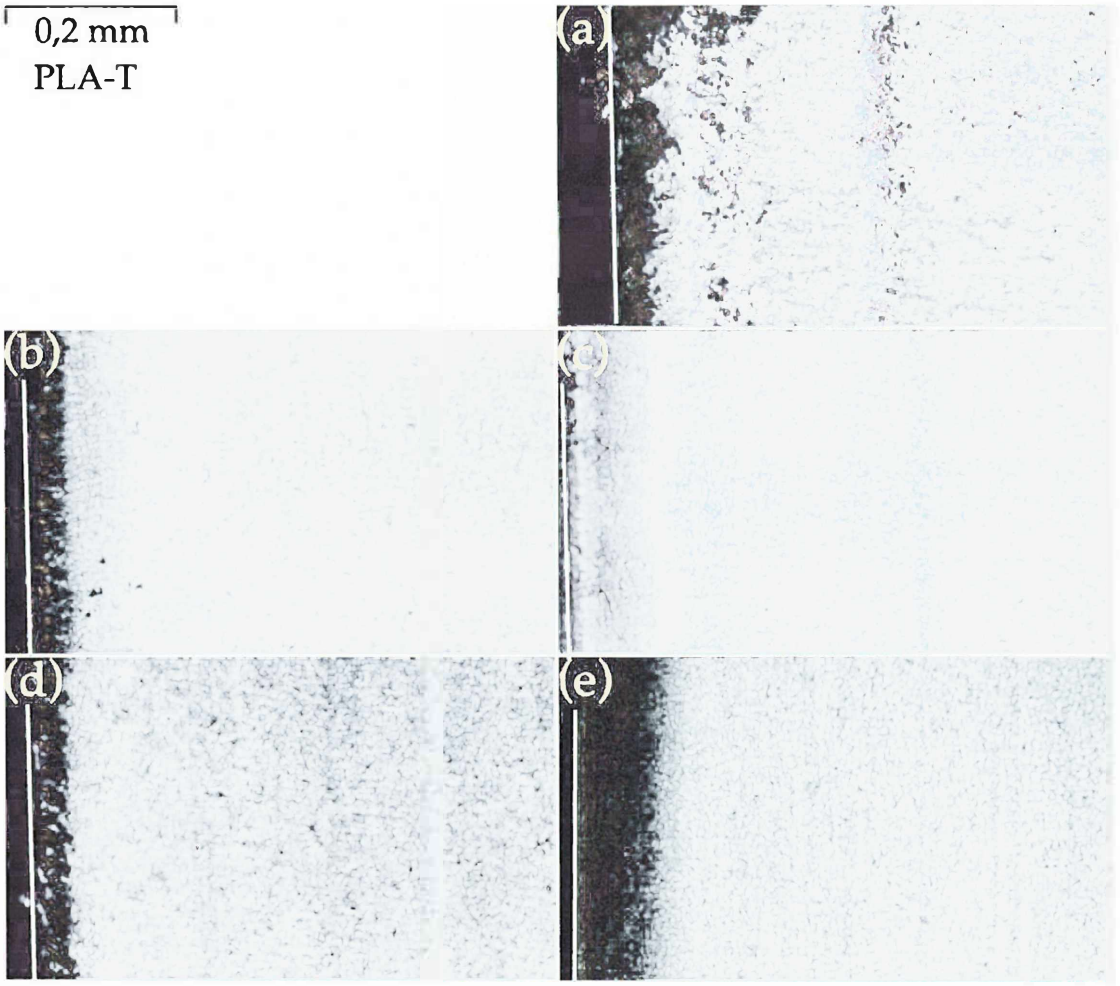

Figure 4.6: Ten times magnified polarized optical micrographs of PLA-T for selected DOE points (a) T1t1, (b) T1t2, (c) T1t3, (d) T3t2, (e) T3t3.

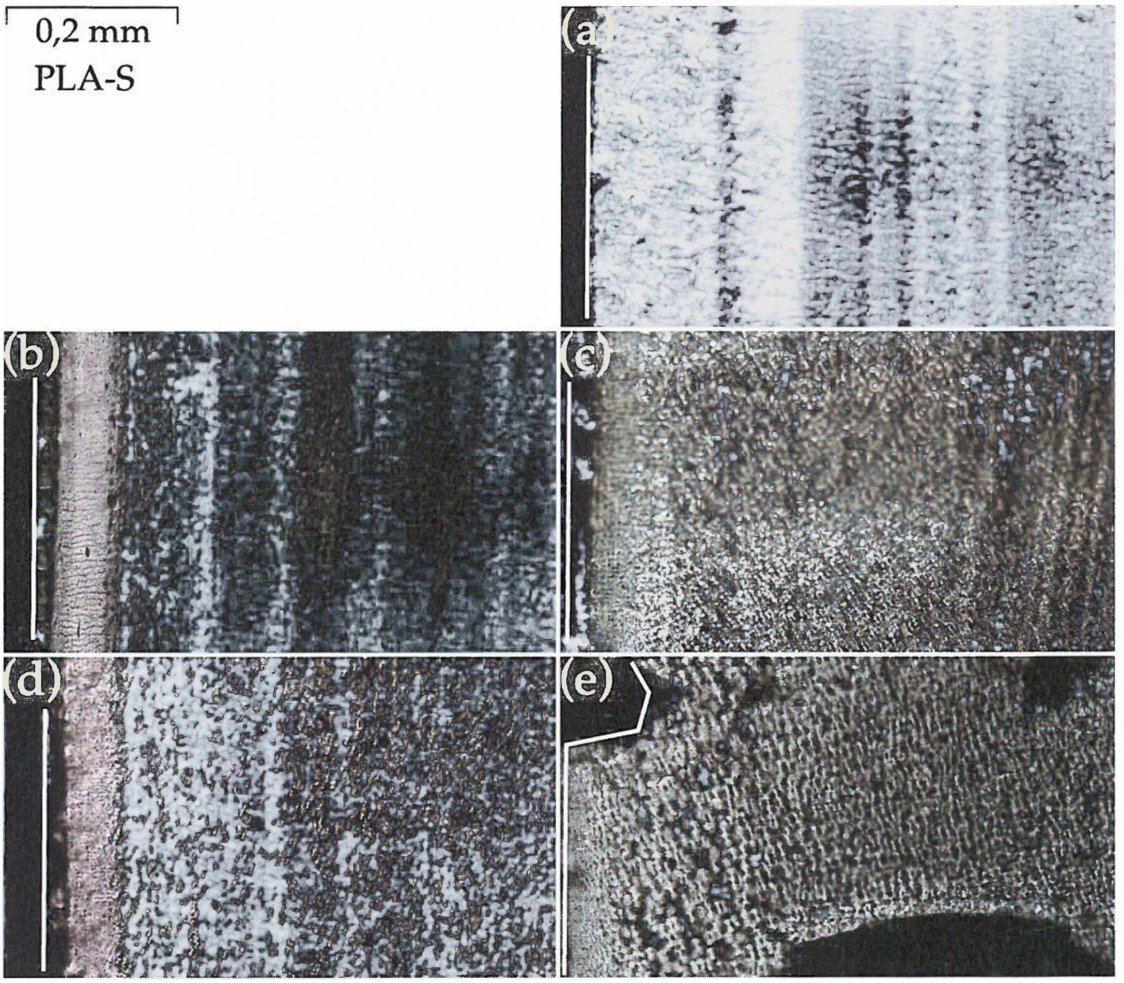

Figure 4.7: Ten times magnified polarized optical micrographs of PLA-S for selected DOE points (a) T1t1, (b) T1t2, (c) T1t3, (d) T3t2, (e) T3t3.

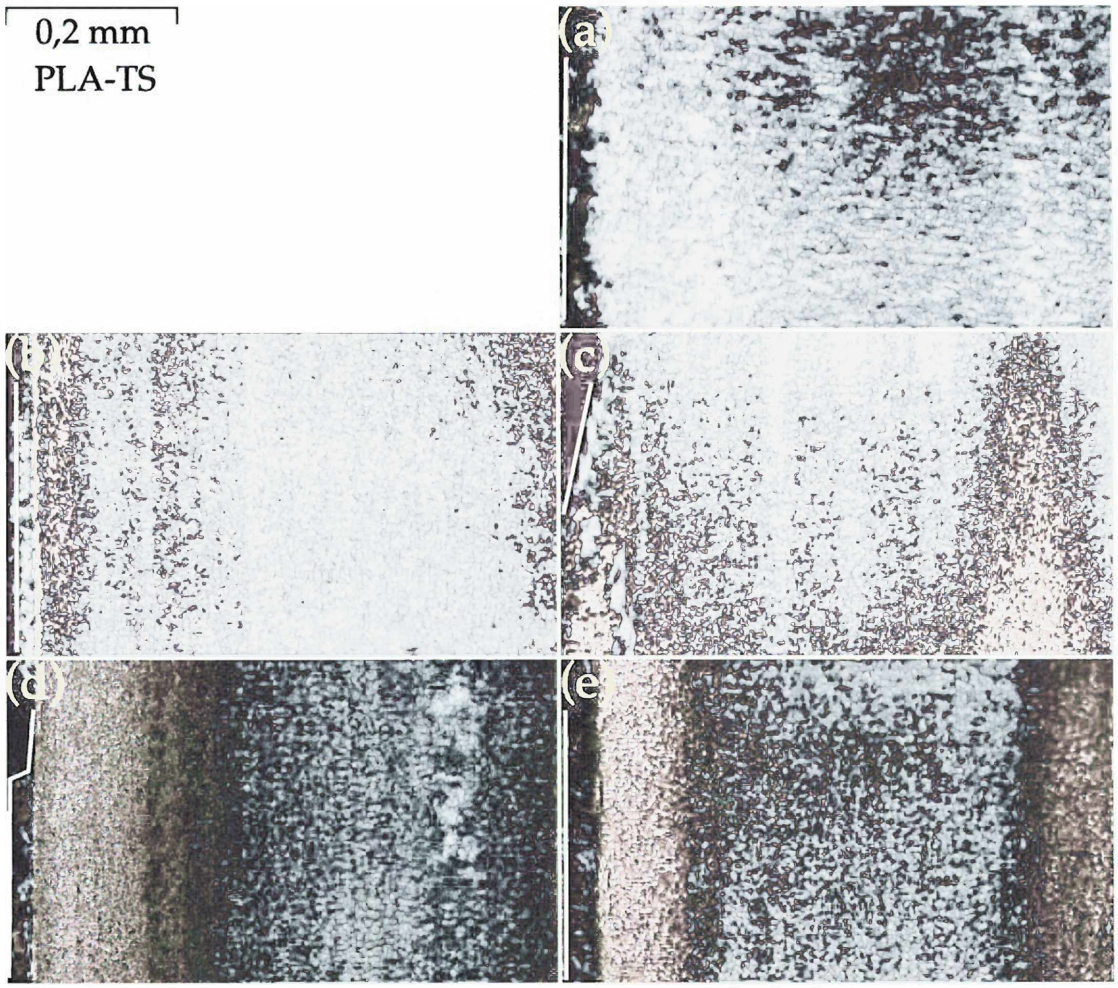

Figure 4.8: Ten times magnified polarized optical micrographs of PLA-TS for selected DOE points (a) T1t1, (b) T1t2, (c) T1t3, (d) T3t2, (e) T3t3.

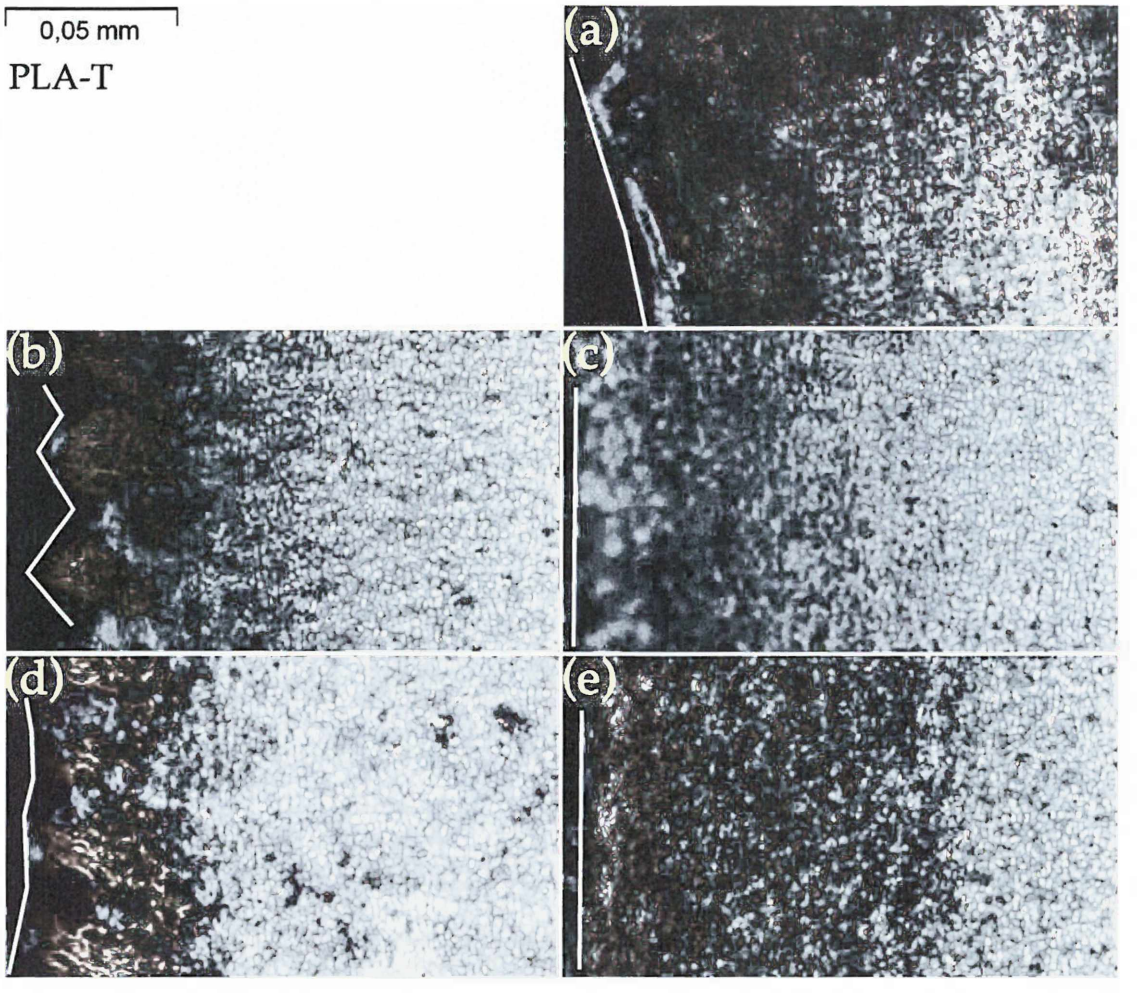

Figure 4.9: 50 times magnified polarized optical micrographs of PLA-T for selected DOE points (a) T1t1, (b) T1t2, (c) T1t3, (d) T3t2, (e) T3t3.

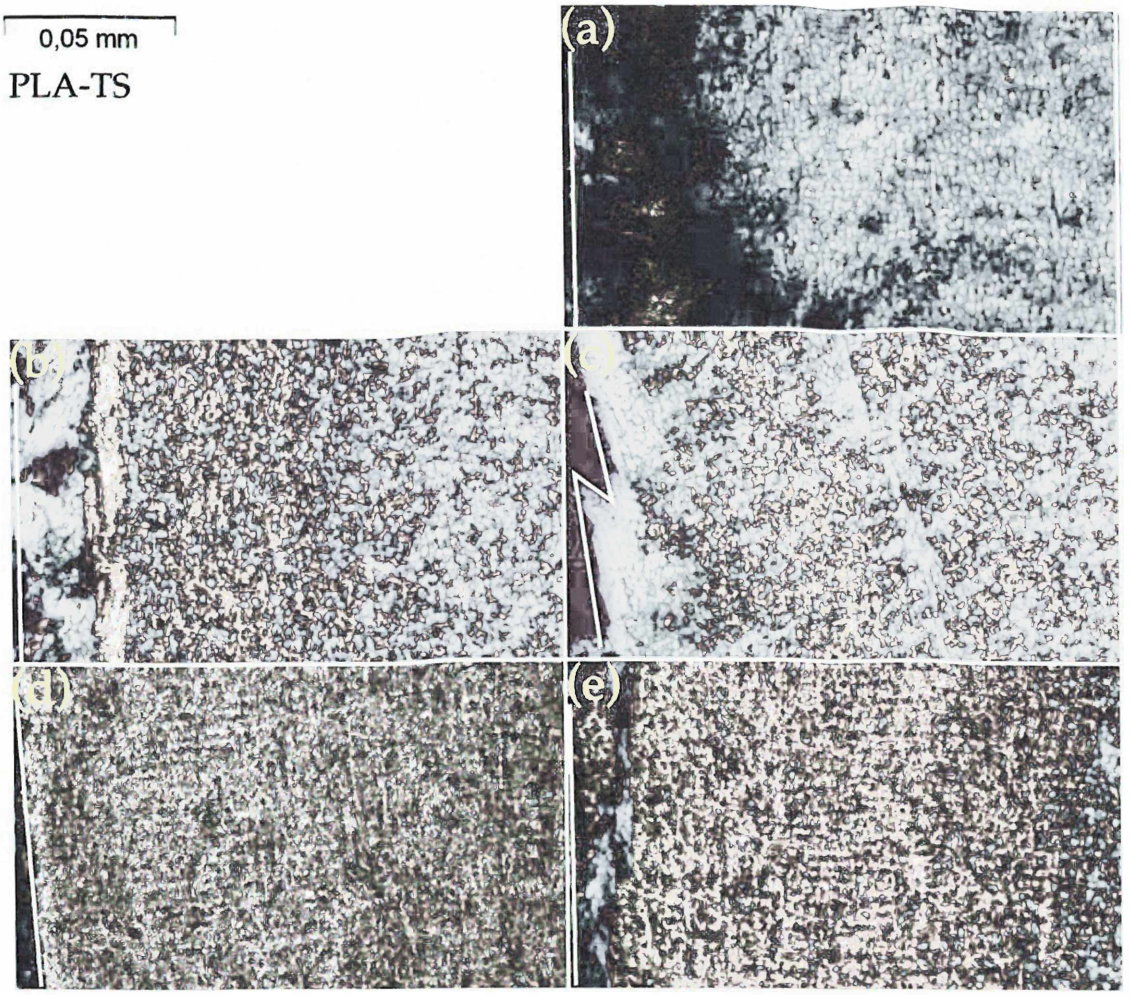

Figure 4.10: 50 times magnified polarized optical micrographs of PLA-TS for selected DOE points (a) T1t1, (b) T1t2, (c) T1t3, (d) T3t2, (e) T3t3.

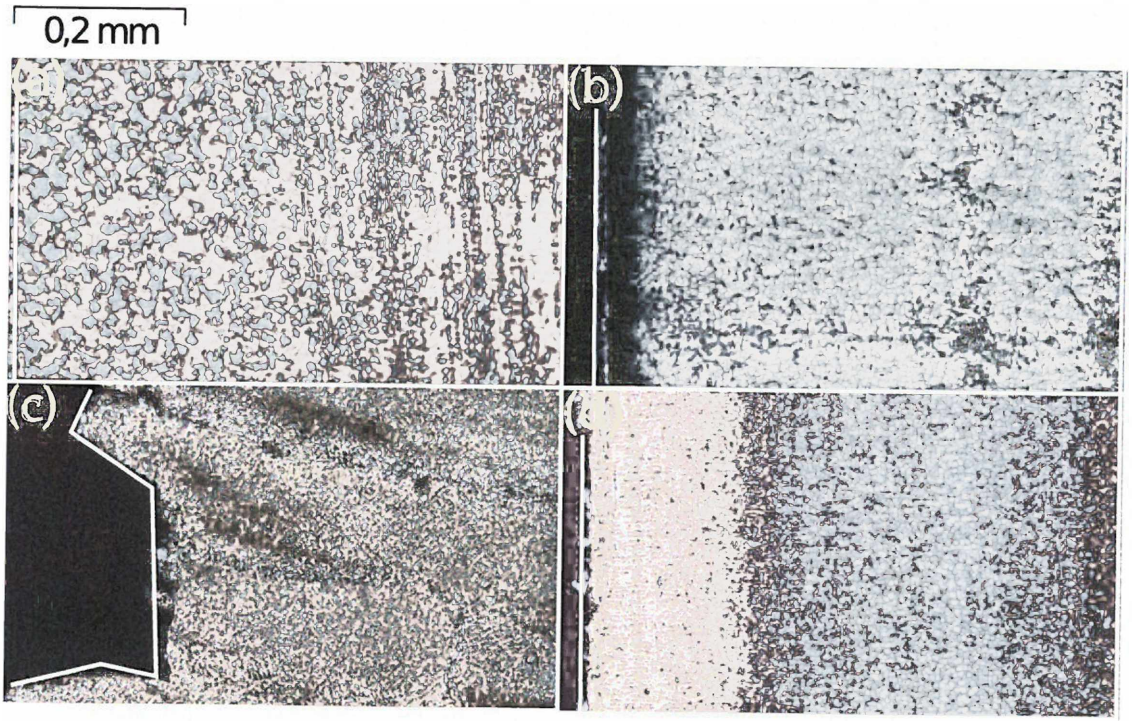

Figure 4.11: Ten times magnified polarized optical micrographs of (a) PLA-N, (b) PLA-T, (c) PLA-S and (d) PLA-TS.

4.3 Thermogravimetrical Analysis (TGA)

Figure 4.12 shows an exemplary TGA scan as well as the derivative of the mass loss for (a) PLA-N and (b) PLA-TS. The derivative of the mass loss during TGA scans is used to detect the degradation of different substances, which show their peak degradation in the same temperature range. PLA-TS contains both filler materials, but only shows one very distinct peak at 368 °C, thus no significant degradation of the filler material occured. The same was also found for PLA-T and PLA-S. It is notable, however, that at the end of the rapid degradation, there is some residue left in the PLA-N scans. This is visible as the mass curve of Figure 4.12 (b) never reaches 0 %, which made a correction of the TGA scans of the compounds necessary. As the PLA-N samples for the TGA analysis were taken straight from the manufacturer, it will be mandatory to check for anorganic components in further investigations. Table 4.4 lists the corrected mean values of anorganic substances left from the compounds as well as the residue from PLA-N scans, which was used for correction.

Table 4.4: TGA scan residue of PLA-N and corrected filler contents of the PLA compounds

PLA-N	PLA-T	PLA-S	PLA-TS
$1,3 \pm 0,2\%$	$5,3 \pm 0,3\%$	$4,7 \pm 0,3\%$	$5,1 \pm 0,3\%$

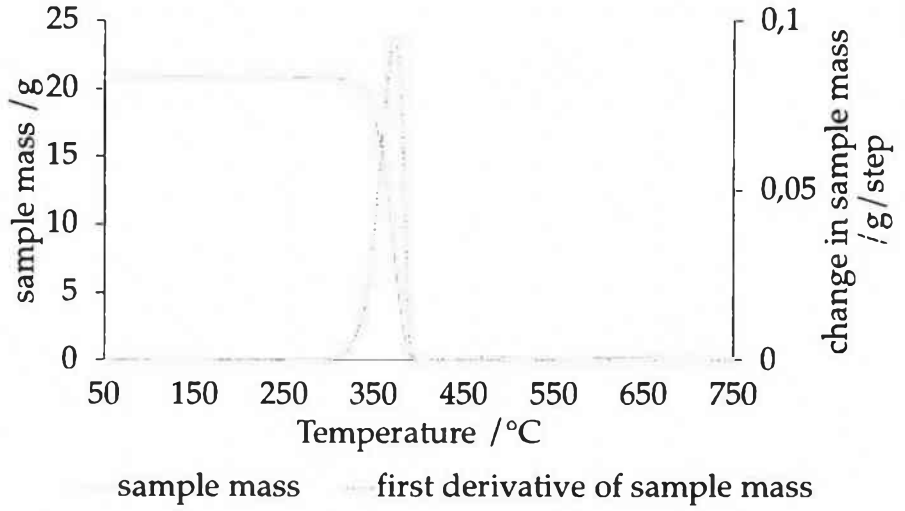

(a)

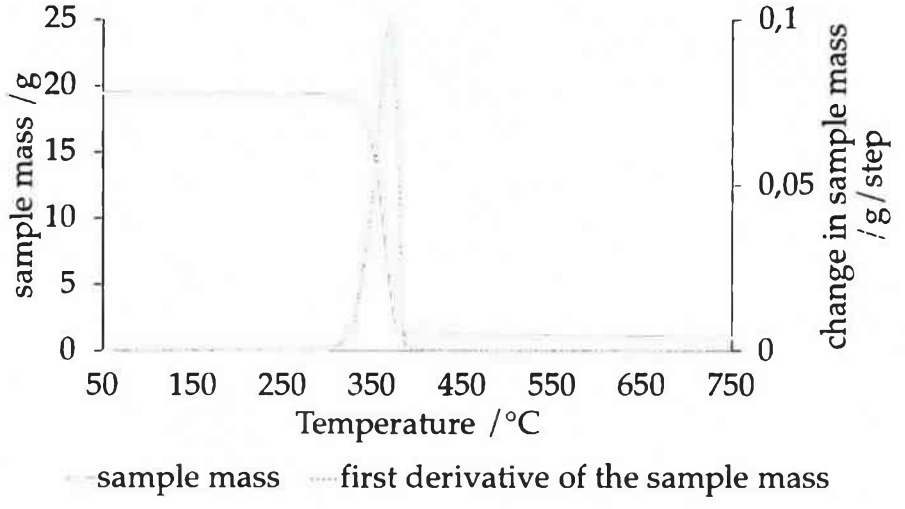

(b)

Figure 4.12: TGA scans and including the first derivative of the mass loss of (a) PLA-N and (b) PLA-TS.

4.4 Hardness

Shore D hardness was also measured at the surface of the injection moulded specimens, right at the same spot were the samples for DSC analysis were taken out. The effect of annealing time on hardness within its prediction bounds is depicted for all used materials in Figure 4.13, where a significant impact of annealing on the surface hardness can be seen, while no significant change in the measured hardness values can be seen between different annealing times or materials.

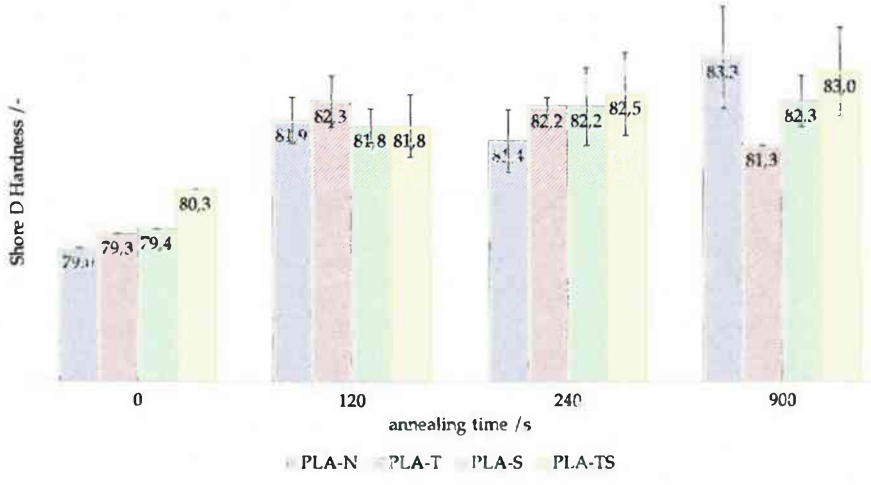

Figure 4.13: Effect of annealing time on Shore D surface hardness of the injection moulded multi-purpose specimens.

5 Discussion

5.1 Analysis of the Repeatability

Since Table 4.3 shows very weak coefficients of determination for all compounds, except PLA-TS, probable causes have to be discussed. As it was shown numerous times, crystallization times of neat PLA tend to be very long. Thus, no significant improvement to the degree of crystallinity was expected to occur for PLA-N within the borders of the chosen DOE [23, 26, 42, 56]. However, Figure 4.5 (d) does show some smaller spherulites, while in Figure 4.5 (e) it is visible that these spherulites did increase in size, but not as much in numbers. Also, for annealing times of 900 s at 120 °, higher degrees of crystallinity than within the DOE could be obtained, which is in good accordance with Crema [56]. While no significant influence on the degree of crystallinity was expected for PLA-N, the nucleated compounds should show a different behaviour [42, 46, 51].

Repeatability of this work could have been negatively influenced by a few key factors. As explained in subsection 3.3.1, there were some issues with the stability of the molding process of specimens out of PLA-T and PLA-S. Mold and injection unit temperatures, which have a far greater influence on crystallinity stayed at their desired levels during the whole manufacturing process and therefore it was chosen to count in specimens of the unstable PLA-T and PLA-S manufacturing process. The DSC sample preparation did not allow for the spatial exactness of sampling, which the inhomogenous distribution of the crystalline areas within the specimens would have required. Figure 5.1 schematically shows the sample preparation process for the DSC samples. However, using a cutter to cut thin slices of material off the sample location as specified in section 3.4 proved to be the best suited method in spite of its

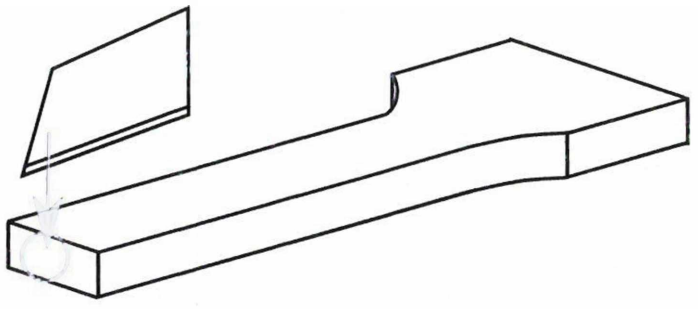

Figure 5.1: Sample preparation process for DSC analysis.

shortcomings. Saws, which could normally provide more accurate cutting, are not suited for DSC sample preparation, because they induce heat, thus altering crystallinity. Other methods would require extensive as well as expensive use of cutting machinery, while still not being able to overcome the problem of inhomogenous distribution of crystalline areas. Perfect sample preparation can lead to deviations of around 0.4 J/g for repeated measurements of heat quantity [62]. For PLA-TS, which showed the most accurate results, standard deviation of the crystal melting heat during the first heating run ranged from 0.2 to 3.2 J/g. In order to get thin enough slices of the required sample weight, it was necessary to cut slices of around one third of the diameter area of the specimens. Plasticised areas induced through cutting can also alter the crystallinity [62]. Little effect on the broad spread of the degree of crystallinity can be accounted to inhomogenous filler distribution, as TGA results showed little deviation of the filler content of the pellets. Additionally, differences between the individual pellets before the injection molding process are balanced out in the bulk material after specimen manufacturing.

All these factors contribute to the relatively high spreading of the degrees of crystallinity obtained via the DSC measurements, which lowers the obtainable coefficients of determination of the fitted surfaces. However, only the prediction of crystallinity of PLA-T is limited by this, since no processing effects on PLA-N were expected and the DSC cooling scans of PLA-S show, there is little nucleating effect of the layered silica. This means, its behaviour should be similar to PLA-N, which it is. For PLA-TS, a good coefficient of correlation could be obtained. This insights can be used to rule out problems, which might occur with further investigations. These investigations could then be used to get more thorough results on the annealing behaviour of specific compounds.

5.2 Effects of the DOE

Figure 5.2 shows very different responses of the different materials to the DOE. While the degree of crystallinity of PLA-N and PLA-S is not significantly influenced by different annealing conditions, PLA-T and PLA-TS show strong responses. While there is no response to the DOE for PLA-S, the overall degree of crystallinity is higher than it is for PLA-N. This weak nucleating effect was unexpected, but is most likely due to subpar exfoliation of the layered silica [47, 49] Lewitus et al. have also used standard twin-screw extruders for compounding, but also could not achieve high levels of exfoliation when mixing the nanoclay directly with the polymer [51]. PLA-T shows a good response to annealing in general, however, higher temperatures and longer annealing times did not lead to a further significant increase in the degree of crystallinity of this compound. Since the degrees of crystallinity of PLA-TS were spread out far closer compared to all other materials, a good fit was achieved (Table 4.3). Figure 5.3 shows the effects for the factors T_a and t_a on the degree of crystallinity for PLA-TS. It can be seen that the biggest step in the degree of crystallinity is when going from no annealing to 120s of annealing. Further annealing does not cause a very significant further increase. While this influence is strictly non linear, annealing temperature has an almost linear effect on the degree of crystallinity, although it is not as strong as the effect of annealing time.

Also, when looking at all the DSC results, it is highly possible that most of the nucleation happening in PLA-TS is caused by the talc, with little influence from the silica. Generally, die polarized optical micrographs of the different materials do substantiate what was found with DSC analysis. PLA-N does not show crystallites at all for T1t1 (Figure 4.5(a)), and only a thin crystallized edge layer at T3t3. Only after 900s of annealing (Figure 4.11, large spherulites have formed throughout a large portion of the diameter. Nucleation in PLA-T and PLA-TS was so effective that spherulites stayed so small, they could only be visualised properly with fifty times magnification (Figure 4.9 and Figure 4.10). This is in good accordance with previous investigations [60].

The optical micrographs of PLA-S (Figure 4.7 do show some effects which can not be determined looking at the DSC charts exclusively. Specimens of this compound do consist

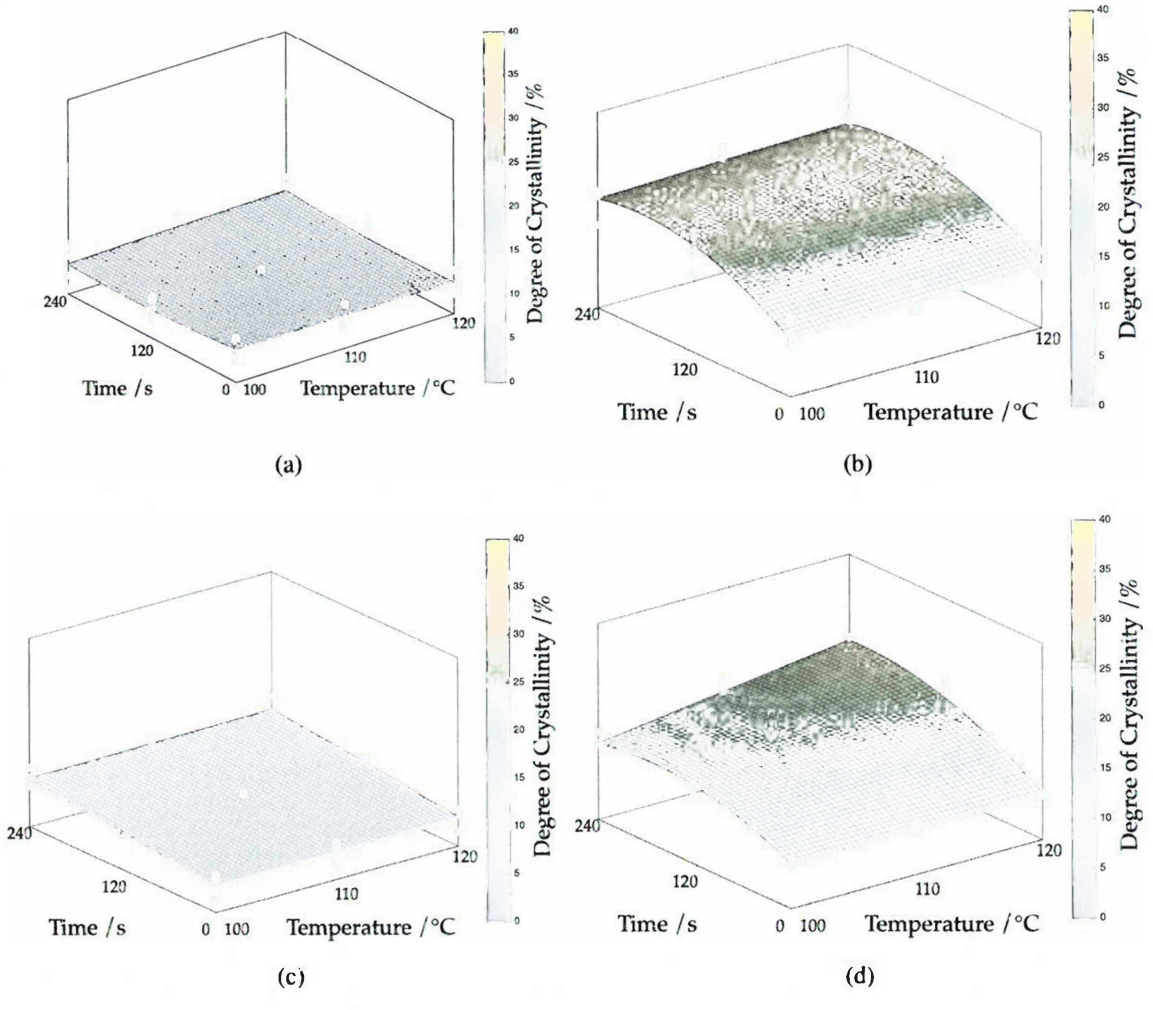

Figure 5.2: Fitted surfaces to the degrees of crystallinity of the different compounds achieved measured via DSC analysis. (a) PLA-N, (b) PLA-T, (c) PLA-S, (d) PLA-TS

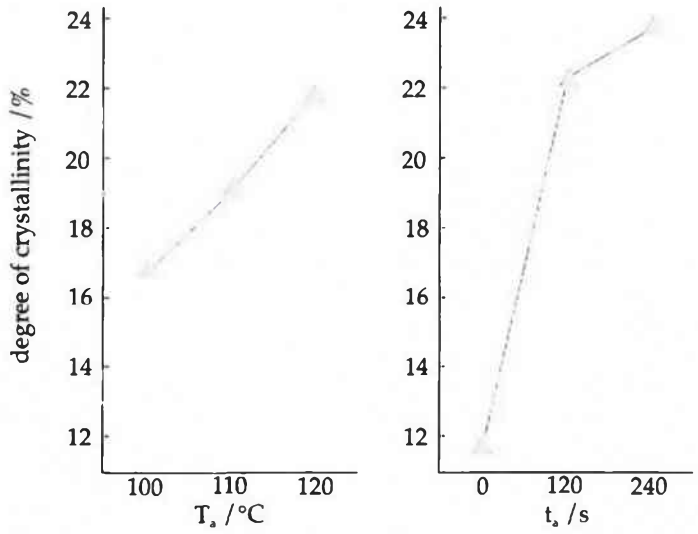

Figure 5.3: Main effects on the crystallinity of PLA-TS as obtained with polynomial surface regression.

of a very brittle border area, which is apparent as a translucent area at the heated edge in Figure 4.7 (b)-(e). It was not possible to perform clean thin cuts of this area without inducing small cracks, which is an indication of high brittleness. It can be seen that this area grows much more with increased annealing time ((b) to (c) respectively (d) to (e)) than with increased temperature ((b) to (d)). This is also backed by the image in Figure 4.11 (c), where it was not possible to get an undestroyed micro cut thin enough to let light through. Previous studies on nanoclay filled PLA have shown strongly reduced elongations at break for tensile testing except for very high levels of exfoliation [66]. This phenomenon can also be found for PLA-TS, although to a lower degree, thus it is very likely caused by the OLMS, and its exact morphology and influence on material properties can be subject to following investigations. When looking more closely at the trends in Shore D hardness (Figure 4.13), it is visible that for all compounds, surface hardness can not be increased by raising the annealing time to the highest settings. Neat PLA, however, has an even higher hardness after 900 s of annealing time, which is in good correlation with Figure 4.11. Overall, despite its limited precision, Shore D Hardness testing shows a good overall correlation with the degree of crystallinity obtained via DSC analysis, as was expected [56].

6 Conclusions

In this work, the applicability of numerous investigations on nucleated PLA compounds under real-world manufacturing conditions has been examined. Talc and layered silica fillers were incorporated into a PLA matrix using a standard corotating twin screw extruder and under water pelletizer. The compounds were investigated regarding the achieved filler content, which was found to be very close to the desired content. From these compounds and the neat PLA, ISO 527 specimens were molded using RHCM technology and a DOE was applied. Those specimens were then investigated regarding their crystallinity via DSC analysis and polarized optical microscopy. It was found that talc is a highly effective filler material which can be incorporated into the polymer with standard equipment. Also, an amount of 5 weight-% of talc is enough to raise crystallinity greatly compared to neat PLA. While the layered silica also acts as a nucleating agent, it is not as ease to incorporate properly into the material. Standard compounding equipment can lead to poor exfoliation of the silica layers, thus limiting the nucleation effect. It was also shown that annealing during the RHCM injection molding process can increase crystallinity even further. While the cycle times used for this investigations are longer than would be required for mass manufacturing, it was shown that when using talc as filler, lower cycle times could also lead to the required increase in degree of crystallinity. An alternative to RHCM process control would be to anneal the parts seperately outside the mold. While this is also viable, there are other limitations. First, annealing times need to be longer, since annealing at over 100 °C outside of a mould can cause unwanted warpage. Second, further investment in parts handling as well as annealing facilities is needed. While RHCM also necessitates investment, it was kept relatively low in this work, as water was used for annealing as well as cooling. Other heating systems like inductive or infrared heating would

require higher investments, but were not needed for the experiments done. When looking at the quality parameters, the filler material can have a negative influence on the process stability, which will require extra care when setting up a production line.

Nomenclature

χ	Degree of Crystallinity
ΔF_D	energy barrier for material transport across the melt/crystal interface
ΔG_V	free energy difference between bulk fluid and bulk crystalline phases
ΔG_r	Gibbs free energy by volume unit
ΔGS	change in Gibbs free energy
ΔH	change in enthalpy
ΔH_V	fusion enthalpy per volume
ψ	apportionment factor
σ	surface energy of the fluid/crystal interface
σ_e	fold surface free energy
I	folded chain nuclei formation rate
I_0	starting rate of formation
k	Boltzmann constant
T_m^0	equilibrium melting temperature
T_a	annealing Temperature
t_a	annealing Time

DOE Design of Experiments

DSC Differential Scanning Calorimetry

OMLS Organically Modified Layered Silicas

PCL polycaprolactone

PDLA Poly(D-lactic acid)

PDLLA Poly(L/D-lactic acid)

PE polyethylene

PET polyethylene terephthalate

PLA poly(lactic acid)

PLLA Poly(L-lactic acid)

PP polypropylene

PS polystyrene

PVA polyvinylalcohol

PVC polyvinylchloride

R^2 coefficient of determination

ROP Ring opening polymerization

S change in entropy

T Temperature

T_c crystallization Temperature

T_g glass transition Temperature

TGA Thermogravimetric Analysis

VST Vicat Softening Temperature

XRD X-ray Diffraction

Bibliography

[1] S. Ebnesajjad. *Handbook of Biopolymers and Biodegradable Plastics*. Elsevier, 2013.

[2] J.-M. Raquez, Y. Habibi, M. Murariu, and P. Dubois. Polylactide (PLA)-based nanocomposites. *Progress in Polymer Science*, 38(10-11):1504–1542, 2013.

[3] S. Sinha Ray and M. Okamoto. Polymer/layered silicate nanocomposites: A review from preparation to processing. *Progress in Polymer Science*, 28(11):1539–1641, 2003.

[4] PlasticsEurope. Plastics- the facts 2012, 2012.

[5] H. J. Endres and A. Siebert-Raths. *Technische Biopolymere*. Hanser, first edition, 2009.

[6] *Allgemeines Umweltaktionsprogramm der Union für die Zeit bis 2020.* Amt für Veröffentlichungen der Europäischen Union, 2014.

[7] Preisentwicklung PP Granulat, 11 2015.

[8] R. Chandra and R. Rustgi. Biodegradable polymers. *Progress in Polymer Science*, 28:1273–1335, 1998.

[9] European Bioplastics. European bioplastics - facts and figures, 2013.

[10] I. Tsiropoulos, A. P. C. Faaij, L. Lunquist, U. Schenker, J. F. Briois, and M. K. Patel. Life cycle impact assessment of bio-based plastics from sugarcane ethanol. *Journal of Cleaner Production*, 90:114–127, 2015.

[11] A. C. Renouf-Glauser, J. Rose, D. Farrar, and R. E. Cameron. A degradation study of PLLA containing lauric acid. *Biomaterials*, 26(15):2415–2422, 2005.

[12] V. Ratta. *Crystallization, Morphology, Thermal Stability and Adhesive Properties of Novel High Performance Semicrystalline Polyimides*. PhD thesis, Virginia Polytechnic Institute and State University, 1999.

[13] A. J. Peacock and A. Calhoun. *Polymer Chemistry*. Hanser, first edition, 2006.

[14] S. P. Parker. *McGraw-Hill Dictionary of Scientific and Technical Terms*. 6. Irwin/Mcgraw Hill, 2002.

[15] J. K. Hobbs. Crystallization kinetics. *Encyclopedia of Polymer Technology*, 2002.

[16] E. W. Fischer, M. Stamm, and M. Dettenmair. Organization of macromolecules in the condensed phase. *Faraday Discussions of the Royal Society of Chemistry*, 68:1–6, 1979.

[17] D. Turnbull and J. C. Fisher. Rate of nucleation in condensed systems. *Journal of Chemical Physics*, 17(1):71–73, 1949.

[18] P. J. Flory. On the morphology of the crystalline state in polymers. *Journal of the American Chemical Society*, 84:2837–2867, 1962.

[19] J. D. Hoffmann, G. T. Davis, and J. I. Lauritzen Jr. *Treatise on Solid State Chemistry-Vol. 3: Crystalline and Noncrystalline Solids, Chapter 3*, volume 3. Plenum Press, 1976.

[20] G. W. Ehrenstein. *Polymerwerkstoffe*. Hanser, third edition, 2011.

[21] A. J. Pennings and M. F. J. Pijpers. On the kinetics of crystallization of polymers from stirred solutions. *Macromolecules*, 3:261–262, 1970.

[22] H. Domininghaus. *Kunststoffe- Eigenschaften und Anwendungen*. Springer, seventh edition, 2008.

[23] R. Auras, L. T. Lim, S. E. M. Selke, and H. Tsuji, editors. *Poly(lactic acid) Synthesis, Structures, Properties, Processing and Application*. Wiley, first edition, 2010.

[24] H. Bannwarth, B. P. Kremer, and A. Schulz. *Basiswissen Physik, Chemie und Biochemie*. Springer, third edition, 2013.

[25] N. Othman, C. Xu, Pa. Mehrkhodavandi, and S. G. Hatzikiriakos. Thermorheological and mechanical behavior of polylactide and its enantiomeric diblock copolymers and blends. *Polymer*, 53(12):2443–2452, 2012.

[26] R. E. Drumright, P. R. Gruber, and D. E. Henton. Polylactic acid technology. *Advanced Materials*, 12:1841–1846, 2000.

[27] L. Cartier, T. Okihara, and B. Lotz. Triangular polymer single crystals: Stereocomplexes, twins and frustrated structures. *Macromolecules*, 30:6313–6322, 1997.

[28] H. Tsuji. Poly(lactide) stereocomplexes: Formation, structure, properties, degradation and application. *Macromolecular Bioscience*, 5, 2005.

[29] Kelly S. Anderson and Marc A. Hillmyer. Melt preparation and nucleation efficiency of polylactide stereocomplex crystallites. *Polymer*, 47(6):2030–2035, 2006.

[30] P. de Santis and A. J. Kovacs. Molecular conformation of poly(s-lactic acid).

[31] M. Cocca, M. L. Di Lorenzo, M. Malinconico, and V. Frezza. Influence of crystal polymorphism on mechanical and barrier properties of poly(l-lactic acid). *European Polymer Journal*, 47(5):1073–1080, 2011.

[32] M. Yasuniwa, S. Tsubakihara, K. Iura, Y. Ono, Y. Dan, and K. Takahashi. Crystallization behavior of poly(l-lactic acid). *Polymer*, 47(21):7554–7563, 2006.

[33] J. Zhang, Y. Duan, H. Sato, H. Tsuji, I. Noda, S. Yan, and Y. Ozaki. Crystal Modifications and Thermal Behavior of Poly(l -lactic acid) Revealed by Infrared Spectroscopy. *Macromolecules*, 38(19):8012–8021, 2005.

[34] B. Eling, S. Gogolewski, and A. J. Pennings. Biodegradable materials of poly(l-lactic acid): 1. melt-spun and solution-spun fibres. *Polymer*, 23:1587–1593, 1982.

[35] D. Sawai, K. Takahashi, T. Imamura, K. Nakamura, T. Kanamoto, and S.H. Hyon. Preparation of oriented beta-form poly(l-lactic acid) by solid-state extrusion. *Journal of Polymer Science Part B: Polymer Physics*, 40:95–104, 2002.

[36] J. Puiggali, Y. Ikada, H. Tsuji, L. Cartier, T. Okihara, and B. Lotz. The frustrated structure of poly(l-lactide). *Polymer*, 41:8921–8930, 2000.

[37] L. Cartier, T. Okihara, Y. Ikada, H. Tsuji, J. Puiggali, and B. Lotz. Epitaxial crystallization and crystalline polymorphism of polylactides. *Polymer*, 41(25):8909–8919, 2000.

[38] L. Wang, Y. Wang, Z. Huang, and Y. Weng. Heat resistance, crystallization behavior, and mechanical properties of polylactide/nucleating agent composites. *Materials & Design*, 66:7–15, 2015.

[39] I. Armentano, N. Bitinis, E. Fortunati, S. Mattioli, N. Rescignano, R. Verdejo, M. A. Lopez-Manchado, and J. M. Kenny. Multifunctional nanostructured PLA materials for packaging and tissue engineering. *Progress in Polymer Science*, 38(10-11):1720–1747, 2013.

[40] H. Bai, C. Huang, H. Xiu, Q. Zhang, and Q. Fu. Enhancing mechanical performance of polylactide by tailoring crystal morphology and lamellae orientation with the aid of nucleating agent. *Polymer*, 55(26):6924–6934, 2014.

[41] D. Battegazzore. Crystallization kinetics of poly(lactic acid)-talc composites. *Express Polymer Letters*, 5(10):849–858, 2011.

[42] H. Li and M. A. Huneault. Effect of nucleation and plasticization on the crystallization of poly(lactic acid). *Polymer*, 48(23):6855–6866, 2007.

[43] T. Ke and X. Sun. Melting behavior and crystallization kinetics of starch and poly(lactic acid) composites. *Journal of Applied Polymer Science*, 89(5):1203–1210, 2003.

[44] J. Cai, M. Liu, L. Wang, K. Yao, S. Li, and H. Xiong. Isothermal crystallization kinetics of thermoplastic starch/poly(lactic acid) composites. *Carbohydrate Polymers*, 86(2):941–947, 2011.

[45] S. Sinha Ray and M. Okamoto. Biodegradable polymers and their layered silicate nanocomposites: In greening the 21st century materials world. *Progress in Materials Science*, 50(8):962–1079, 2005.

[46] S. Sinha Ray, K. Yamada, M. Okamoto, Y. Fujimoto, A. Ogami, and K. Ueda. New polylactide/layered silicate nanocomposites. 5. Designing of materials with desired properties. *Polymer*, 44(21):6633–6646, 2003.

[47] M. Alexandre and P. Dubois. Polymer-layered silicate nanocomposites: Preparation, properties and uses of a new class of materials. *Materials Science and Engineering: R: Reports*, 28(1-2):1–63, 2000.

[48] S. Sinha Ray, P. Maiti, M. Okamoto, K. Yamada, and K. Ueda. New polylactide/layered silicate nanocomposites. 1. Preparation, Characterization and Properties. *Macromolecules*, 35:3104–3110, 2002.

[49] Y. Di, S. Iannace, E. Di Maio, and L. Nicolais. Poly(lactic acid)/organoclay nanocomposites: Thermal, rheological properties and foam processing. *Journal of Polymer Science Part B: Polymer Physics*, 43(6):689–698, 2005.

[50] J. Y. Nam, S. Sinha Ray, and M. Okamoto. Crystallization behavior and morphology of biodegradable polylactide/layered silicate nanocomposite. *Macromolecules*, 36(19):7126–7131, 2003.

[51] D. Lewitus, S. McCarthy, A. Ophir, and S. Kenig. The effect of nanoclays on the properties of PLLA-modified polymers part 1: Mechanical and thermal properties. *Journal of Polymers and the Environment*, 14:171–177, 2006.

[52] J. Rhim, S. Hong, and C. Ha. Tensile, water vapor barrier and antimicrobial properties of PLA/nanoclay composite films. *LWT - Food Science and Technology*, 42(2):612–617, 2009.

[53] R. Homklin and N. Hongsriphan. Mechanical and thermal properties of pla/pbs co-continuous blends adding nucleating agent. *Energy Procedia*, 34:871–879, 2013.

[54] P.D. Haaland. *Experimental design in biotechnology*. Marcel Dekker, Inc, first edition, 1989.

[55] E. Rosales, M. A. Sanromán, and M. Pazos. Application of central composite face-centered design and response surface methodology for the optimization of electro-fenton decolorization of azure b dye. *Environmental Science and Pollution Research*, 19:1738–1746, 2012.

[56] L. Crema. *A study of rapid mould temperature variation influence on morphology and appearance of injection moulded parts.* PhD thesis, Universita degli studi di Padova, Padova, 2015.

[57] J. F. Turner, A. Riga, A. O'Connor, J. Zhang, and J. Collis. Characterization of drawn and undrawn poly-l-lactide films by differential scanning calorimetry. *Journal of Thermal Analysis and Calorimetry*, 75:257–268, 2004.

[58] W. Grellmann and S. Seidler, editors. *Polymer Testing*. Hanser, second edition, 2013.

[59] B. Kalb and A. J. Pennings. General crystallization behaviour of poly(l-lactic acid). *Polymer*, 21(6):607–612, 1980.

[60] Z. Refaa, M. Boutaous, F. Rousset, R. Fulchiron, M. Zinet, S. Xin, and P. Bourgin. Crystallization kinetics of poly-(lactic acid) with and without talc: Optical microscopy and calorimetric analysis. *AIP Conference Proceedings*, 1593:342–346, 2014.

[61] C. Y. Hung, C. C. Wang, and C. Y. Chen. Enhanced the thermal stability and crystallinity of polylactic acid (PLA) by incorporated reactive PS-b-PMMA-b-PGMA and PS-b-PGMA block copolymers as chain extenders. *Polymer*, 54(7):1860–1866, 2013.

[62] A. Frick and C. Stern. *DSC-Prüfung in der Anwendung*. Hanser, first edition, 2006.

[63] M. Yasuniwa, K. Iura, and Y. Dan. Melting behavior of poly(l-lactic acid): Effects of crystallization temperature and time. *Polymer*, 48(18):5398–5407, 2007.

[64] T. F. Cipriano and A. L. N. da Silva. Thermal, rheological and morphological properties of poly(lactic acid) (PLA) and talc composites. *Polímeros*, 24(3):276–282, 2014.

[65] M. Yasuniwa, S. Tsubakihara, and T. Fujioka. X-ray and DSC studies on the melt-recrystallization process of poly(butylene naphthalate). *Thermochimica Acta*, 396:75–78, 2003.

[66] J.-W. Huang, Y. C. Hung, Y.-L. Wen, C.-C. Kang, and M.-Y. Yeh. Polylactide/nano and microscale silica composite films. i. preparation and characterization. *Journal of Applied Polymer Science*, 112:1688–1694, 2009.